Combined α- and β-adrenergic receptor activation triggers thermogenesis by the futile creatine cycle

Lawrence Kazak (lawrence.kazak@mcgill.ca)
McGill University https://orcid.org/0000-0002-7591-2544

Janane Rahbani
McGill University https://orcid.org/0000-0003-4598-4683

Charlotte Scholtes
McGill University

Damien Lagarde
McGill University

Mohammed Faiz Hussain
McGill University

Anna Roesler
McGill University

Christien Dykstra
McGill University

Jakub Bunk
McGill University

Bozena Samborska
McGill University

Shannon O'Brien
University of Birmingham

Emma Tripp
University of Birmingham https://orcid.org/0000-0003-1425-5541

Alain Pacis
McGill University

Anthony Angueira
University of Pennsylvania

Olivia Sveidahl Johansen
University of Copenhagen

Jessica Cinkornpumin
McGill University

Ishtiaque Hossain
McGill University

Matthew Lynes

Maine Medical Center Research Institute https://orcid.org/0000-0003-0746-0854
Yang Zhang
Harvard Medical School
Andrew White
Harvard Medical School
William Pastor
McGill https://orcid.org/0000-0003-4176-5299
Maria Chondronikola
University of California
Labros Sidossis
Rutgers University
Samuel Klein
Washington University School of Medicine and Sansum Diabetes Research Institute
Anastasia Kralli
Johns Hopkins
Aaron Cypess
National Institute of Diabetes and Digestive and Kidney Diseases https://orcid.org/0000-0002-5570-9346
Steen Pedersen
Aarhus University Hospital https://orcid.org/0000-0002-7838-8063
Niels Jessen
Department of Biomedicine, Aarhus University https://orcid.org/0000-0001-5613-7274
Yu-Hua Tseng
Joslin Diabetes Center/Harvard Medical School https://orcid.org/0000-0003-2053-9559
Zachary Gerhart-Hines
University of Copenhagen
Patrick Seale
University of Pennsylvania https://orcid.org/0000-0001-7119-1615
Davide Calebiro
University of Birmingham https://orcid.org/0000-0002-3811-1553
Vincent Giguere
McGill University https://orcid.org/0000-0001-9567-3694

Biological Sciences - Article

Keywords:

Posted Date: January 17th, 2022

DOI: https://doi.org/10.21203/rs.3.rs-1190032/v1

Abstract

Noradrenaline is the primary physiological regulator of adipocyte thermogenesis in response to decreased environmental temperature[1]. However, the molecular factors and effector pathways that lie downstream of noradrenaline-stimulated thermogenesis are still not fully understood but are purportedly driven by cAMP downstream of β-adrenergic receptor (βAR) activation. Furthermore, while the transcriptional mechanisms regulating Ucp1 are well-characterized[2], the transcriptional regulation of UCP1-independent thermogenesis is largely unknown. Here, we show that brown adipose tissue (BAT) is primed to respond to environmental cold by triggering coordinated α-adrenergic receptor (αAR) and βAR signaling to induce the expression of thermogenic genes of the futile creatine cycle[3,4]. Using fat-specific loss-of-function models, we reveal that EBFs, ERRs, and PGC1α are required for the cold-stimulated transcriptional induction of the futile creatine cycle in vivo. Through the application of chemogenetics, we demonstrate that combined fat-selective Gαs (activated by βARs) and Gαq (activated by αARs) signaling elevates whole-body energy expenditure to a greater extent than either signaling pathway alone in a manner that is dependent on the key effector protein of the futile creatine cycle, CKB[3]. Moreover, genetic and pharmacological studies reveal that CKB is necessary for nearly all of the α_1AR-stimulated component of brown adipocyte-intrinsic respiration and is thus critical for the full activation of noradrenaline-stimulated thermogenesis. Thus, the futile creatine cycle is integrated into facultative and adaptive thermogenesis through coordinated α_1AR and β_3AR signaling.

Main Text

The physiological activation of adipocyte thermogenesis is mediated by the sympathetic nervous system via the release of noradrenaline (NA) from nerve terminals directly innervating thermogenic adipocytes[5-9]. NA elicits the full thermogenic response of brown adipocytes via both facultative and adaptive mechanisms[10]. Facultative mechanisms utilize the effector pathways that are poised to promote rapid activation of thermogenesis upon demand, whereas adaptive processes involve the induction of thermogenic gene expression and adipogenesis[2,11,12]. In this regard, b-adrenergic receptor (bAR) signaling has received the most attention[13-15]. The bAR cascade signals through Ga_s to stimulate the cyclic AMP (cAMP)-dependent pathway to induce macronutrient oxidation and thermogenesis[16-20]. However, although it has long been appreciated that NA engages G protein-coupled receptors (GPCRs) aside from bARs on brown adipocytes[21], the involved effector pathways contributing to NA-stimulated adipocyte thermogenesis are still not fully understood.

The a-adrenergic receptor, *Adra1a*, is enriched in BAT

Since much of adipocyte thermogenesis is regulated by the sympathetic nervous system through GPCR signaling in brown adipocytes[13,14,22], we analyzed ribosomal profiling data[23] to score GPCR mRNA expression based on two properties: (1) mRNA enrichment in brown adipose tissue (BAT) and (2) mRNA abundance in BAT (10% most abundant GPCRs). Four genes (*Adra1a*, *Adrb1*, *Ptger1* and *Cxcr7*) fulfilled

these criteria (Extended Data Fig. 1a). Analysis of an independent mouse ribosomal profiling dataset[24] confirmed BAT-enrichment of *Adra1a*, *Adrb1* and *Cxcr7 (Ptger1* was not identified) (Extended Data Fig. 1b). *Adra1a* was the most abundant a_1AR subtype in murine brown adipocytes, followed by *Adra1d*, whereas *Adra1b* and all the a_2AR subtypes were poorly expressed (Extended Data Fig. 1c). Of the GPCR candidates, *ADRA1A* was the most enriched in human deep BAT (proximal to the carotid sheath) over paired white subcutaneous adipose tissue (SAT) (Fig. 1a), followed by *ADRB1* (Extended Data Fig. 1d), while *PTGER1* and *CXCR7* did not exhibit BAT enrichment (Extended Data Fig. 1e, f). RNA sequencing (RNA-seq) analysis of an independent human cohort revealed that *ADRA1A* displayed the highest expression levels in supraclavicular adipose tissue (primary location of human BAT) compared to all aARs and bARs (Extended Data Fig. 1g). Together, these data prompted us to focus our attention on aAR signaling in BAT.

aAR signaling regulates futile creatine cycling gene expression in BAT

To explore the cold-stimulated transcriptional program regulated by aAR signaling, we generated RNA-seq transcriptomes from BAT of mice pre-treated with either a single intraperitoneal (i.p.) injection of the aAR antagonist phenoxybenzamine (PBZ) or saline control and then housed at 30°C or 6°C (Fig. 1b). Principal component analysis of gene expression showed that ~65% of variation (PC1) was explained by temperature and ~15% of variation (PC2) was sensitive to aAR antagonism (Extended Data Fig. 2a). PBZ treatment essentially had no effect on gene expression at 30°C (Fig. 1b and Extended Data Fig. 2b, c). We identified four gene clusters stratified by differential expression profiles (Fig. 1b and Extended Data Table 1). Cluster 4 was defined by cold-induced genes that were reduced in abundance by PBZ treatment (Fig. 1b). Analysis of this gene set revealed significant GO term pathway enrichment of protein transmembrane import into organelle and protein translocation to mitochondria, among others (Extended Data Fig. 2d). Notably, mRNAs encoding the effector proteins of the futile creatine cycle: creatine kinase b (*Ckb*)[3] and tissue-nonspecific alkaline phosphatase (*Alpl,* encoding TNAP)[4] were cold-inducible in a PBZ-dependent manner. Similarly, peroxisome proliferator-activated receptor gamma co-activator 1 (*Ppargc1a*) mRNA, encoding for PGC1α, a key transcriptional co-activator of mitochondrial and thermogenic genes[25,26], was a cold-stimulated PBZ target (Extended Data Table 1). In a separate mouse cohort, both PBZ and a structurally distinct a_1AR-specific antagonist, prazosin (PZS) inhibited the cold-stimulated induction of *Ckb*, *Alpl* and *Ppargc1a* in BAT (Extended Data Fig. 2e). Both PBZ and PZS blunted the cold-stimulated induction of CKB protein in BAT (Fig. 1c and Extended Data Fig. 2f). In contrast, uncoupling protein 1 (*Ucp1*) mRNA and protein levels were unchanged by pharmacological aAR antagonism (Fig. 1c and Extended Data Fig. 2e, f). Next, we carried out unilateral denervation of the interscapular BAT depot in which the right lobe was surgically denervated while the left lobe remained intact[22]. Strikingly, the cold-mediated elevation of *Ckb*, *Alpl* and *Ppargc1a* was blocked in the sympathetically denervated BAT lobes (Fig. 1d) demonstrating that innervation of BAT by the sympathetic nervous system is required to elevate futile creatine cycling genes in response to cold. Of note, even though *Adrb1* was BAT-enriched (Extended Data Fig. 1a, d), ADRB1-dependent regulation of futile creatine cycling gene expression was ruled out because either genetic ablation of *Adrb1* or

pharmacological inhibition with propranolol did not block cold-stimulated *Ckb*, *Alpl* and *Ppargc1a* mRNA induction or CKB protein induction in BAT (Extended Data Fig. 3a-d). Finally, *ADRA1A* was positively correlated with *CKB* in multiple independent human BAT cohorts (Fig. 1e and Extended Data Fig. 3e-g). In contrast, *CKB* did not display a positive correlation with *ADRA1A* in SAT (Extended Data Fig. 3h, i) or consistent associations with *ADRB1*, *PTGER1* or *CXCR7* in BAT (Extended Data Fig. 3j). Collectively, these data suggest that the cold-stimulated elevation of futile creatine cycling genes is regulated, at least in part, by the sympathetic nervous system through aAR signaling in BAT.

BAT is primed to induce CKB by aAR and b_3AR signaling

Like *ADRA1A*, *ADRB3* was positively correlated with *CKB* in human BAT (Extended Data Fig. 4a, b). This was consistent with the capacity for pharmacological b_3AR activation (by CL 316,243) to increase CKB protein in murine BAT (Extended Data Fig. 4c). b_3AR-stimulated induction of *Ckb*, *Alpl*, *Ppargc1a*, and *Ucp1* mRNA and CKB, TNAP and UCP1 protein levels were not blocked by PBZ (Extended Data Fig. 4c, d), indicating that PBZ did not indirectly effect b_3AR-stimulated thermogenic gene induction. We did not detect any difference in the amount of *Ckb* (or *Alpl* and *Ucp1*) induction if CL 316,243 was administered by daily i.p. injection or by continuous release through an osmotic pump (Extended Data Fig. 4e), suggesting that the induction of *Ckb* by individual b_3AR stimulation occurs similarly whether stimulated transiently or continuously. However, the cold-stimulated induction of *Ckb* in BAT was higher (about 12-fold) than b_3AR agonism (about 4.5-fold), whereas the induction of *Ucp1* mRNA expression by these interventions was comparable (Extended Data Fig. 4g). Finally, *Ckb* levels in BAT following b_3AR activation (Extended Data Fig. 4d) mirrored the remaining levels of *Ckb* in aAR-inhibited cold-activated BAT (Extended Data Fig. 4f), suggesting that the residual cold-stimulated induction of *Ckb* during aAR blockade was mediated by the b_3AR pathway. Cold exposure or b_3AR agonism both elicited a greater relative induction of *Ckb* mRNA and protein in BAT compared to SAT (Fig. 1h and Extended Data Fig. 4g-j), even though b_3AR expression was comparable between these tissues (Extended Data Fig. 4k)[23]. These data indicate that in addition to BAT-selective aAR signaling, intracellular factors contribute towards the priming of brown adipocytes to trigger CKB expression downstream of b_3AR signaling. Of note, CKB abundance was substantially induced in SAT following 1 week of cold exposure (Extended Data Fig. 4l), suggesting that its expression was commensurate with beige adipogenesis. In aggregate, our data suggest that BAT is equipped to rapidly induce CKB expression in response to external adrenergic stimuli through combined a_1AR and b_3AR signaling.

Transcriptional regulation of the futile creatine cycle

Using ATAC (assay for transposase-accessible chromatin) sequencing of BAT nuclei, we identified differentially accessible regions (DARs) proximal to the differentially expressed genes of our BAT transcriptomes (Fig. 2a). We next identified transcription factor motifs which were: (1) statistically enriched in DARs proximal to Cluster 4 genes and (2) present in cold-stimulated DARs proximal to both *Ckb* and *Alpl* (Fig. 2b). We found ERR (estrogen-related receptor) and EBF (early B-cell factor) response

elements to be most enriched (Fig. 2c). ERRα and its co-activator partner PGC1α are known transcriptional regulators of the cold response[26,27], and EBF2 facilitates the binding of ERRα and PGC1α on target thermogenic genes[26,28]. Thus, we explored the chromatin occupancy of ERRα at the cold-responsive DARs of *Ckb* and *Alpl* in BAT (Fig. 2b) using chromatin immunoprecipitation coupled to qPCR (ChIP-qPCR). At 30ºC, ERRα binding to DARs proximal to both *Ckb* and *Alpl* was enriched (by about 4-fold) over a control region that is not bound by ERRα (Fig. 2d, e and Extended Data Fig. 5). 6ºC exposure further enhanced the occupancy of ERRα (by about 2-fold over 30ºC) on all cold-responsive DARs proximal to *Ckb* containing ERR motifs (Fig. 2d, e). In contrast, ERRα binding to cold-triggered DARs proximal to *Alpl* was not cold-inducible (Extended Data Fig. 5). PBZ did not alter chromatin accessibility (Fig. 2a, b) or ERRα occupancy on DARs proximal to *Ckb* and *Alpl* (Fig. 2d, e and Extended Data Fig. 5), indicating that antagonism of aAR signaling during cold exposure does not influence chromatin binding activity.

Next, we sought to determine if ERR, EBF, and PGC1a regulate futile creatine cycling gene expression in BAT *in vivo*. *Esrrg* (ERRg) can compensate for loss of *Esrra* (ERRα)[27] and *Ebf1* can compensate for loss of *Ebf2*[26]. Thus, we utilized mice with adipocyte-selective double deletion of either *Esrra*/*Esrrg* (*Esrra*/*g*^{AdipoqCre})[27] or *Ebf1*/*Ebf2* (*Ebf1/2*^{AdipoqCre})[26]. Strikingly, upon loss of either *Esrra*/*Esrrg* (Extended Data Fig. 6a) or *Ebf1/Ebf2* (Extended Data Fig. 6b) the cold-induced increase of *Ckb* mRNA in BAT was fully blocked (Fig. 2f, g). The cold-stimulated induction of CKB protein was also fully dependent on *Esrra*/*Esrrg* (Extended Data Fig. 6c). The induction of *Alpl* mRNA by cold was completely inhibited upon loss of *Ebf1/Ebf2* (Fig. 2g); however, the cold-stimulated increase of *Alpl* mRNA was *Esrra*/*Esrrg*-independent (Fig. 2f), fully consistent with our ChIP-qPCR analysis (Extended Data Fig. 5). Surprisingly, the elevation of *Ucp1* mRNA and protein by cold was also independent of *Esrra*/*Esrrg* (Fig. 2f and Extended Data Fig. 6c). We discovered that *Ppargc1a* and *Alpl* were both induced to a higher level in BAT of cold-exposed *Esrra*/*g*^{AdipoqCre} compared to control mice (Fig. 2f and Extended Data Fig. 6a). Thus, because *Ppargc1a* and *Alpl* mirrored one another upon cold exposure in *Esrra*/*g*^{AdipoqCre} mice, and because *Ckb, Alpl*, and *Ppargc1a* levels were all similarly regulated by aAR signaling (Fig. 1c, d), we hypothesized that futile creatine cycling gene expression is regulated by PGC1a. To test this hypothesis, we constructed mice with selective and inducible deletion of *Ppargc1a* in *Ucp1*$^{+}$ cells (*Ppargc1a*^{Ucp1CreERT2}) to avoid possible developmental effects associated with chronic *Ppargc1a* deletion. Tamoxifen-mediated reduction of *Ppargc1a* in this model exhibited a similar level of diminution as with aAR antagonism, while *Ebf1, Ebf2*, *Esrra,* and *Esrrg* levels were not reduced (Extended Data Fig. 6d). Strikingly, genetic depletion of *Ppargc1a* significantly diminished the cold-stimulated induction of both *Ckb* (by about 65%) and *Alpl* (by about 45%) mRNA (Fig. 2h) and CKB and TNAP protein (Fig. 2i and Extended Data Fig. 6e). Similarly, the b_3AR-stimulated induction of both CKB and TNAP was reduced in BAT of *Ppargc1a*^{Ucp1CreERT2} compared to *Ppargc1a*$^{fl/fl}$ mice (Extended Data Fig. 6f). Surprisingly, *Ppargc1a* was dispensable for the induction of *Ucp1* mRNA and protein by cold exposure (Fig. 2h and Extended Data Fig. 6f). Together, our findings show that the expression of both *Ckb* and *Alpl* is dependent on *Ebf1*/*Ebf2* and *Ppargc1a* in brown adipocytes in response to cold. However, while *Ckb* expression by

cold depends on *Esrra*/*Esrrg*, cold-stimulated *Alpl* expression is *Esrra*/*Esrrg*-independent and transcriptionally regulated by factors that remain to be defined. Thus, our data is consistent with a model where PGC1a abundance is regulated by environmental cold through combined a_1AR and b_3AR signaling to control futile creatine cycling gene expression in brown adipocytes (Fig. 2j).

NA-stimulated thermogenesis requires a_1AR signaling and CKB

GPCR signaling regulates both the acute activation of thermogenesis and the reconfiguring of transcriptional networks to support enhanced catabolic demand[22,27,29-31]. Since our data suggested that cold-stimulated aAR stimulation is required for maximal induction of *Ckb* expression, we explored the possibility that facultative thermogenesis downstream of NA-stimulated aAR signaling requires *Ckb*. First, we injected mice with NA which stimulated an increase in whole-body energy expenditure above the stress response elicited by saline injections, and notably was significantly decreased in fat-selective *Ckb* knockout mice ($Ckb^{AdipoqCre}$) compared to control $Ckb^{fl/fl}$ mice (Fig. 3a, b). These data are consistent with the recently established role for CKB in thermogenesis by the futile creatine cycle[3]. However, given that activation of adrenergic signaling by NA is not confined to fat, it was critical to delineate the brown adipocyte-intrinsic regulation of NA-stimulated respiration by *Ckb* and aAR signaling (Fig. 3c). Importantly, the NA-stimulated rise in respiration of freshly isolated $Ckb^{AdipoqCre}$ interscapular brown adipocytes was significantly impaired (by about 45%) compared to $Ckb^{fl/fl}$ brown adipocytes (Fig. 3d, e), recapitulating our *in vivo* data. Moreover, inhibition of aAR signaling reduced NA-dependent respiration of $Ckb^{fl/fl}$ control brown adipocytes, without statistically altering $Ckb^{AdipoqCre}$ brown adipocyte respiration (Fig. 3d, e). *Ckb* deficiency or aAR inhibition had no effect on unstimulated (basal) respiration (Extended Data Fig. 7a), consistent with a role for CKB in facultative thermogenesis. CKB deficiency or aAR antagonism had no effect on NA-stimulated lipolysis (Extended Data Fig. 7b), indicating that the diminished capacity of $Ckb^{AdipoqCre}$ brown adipocytes to trigger adrenergic-stimulated thermogenesis could not be explained by reduced substrate delivery. Repeating the experiments with PZS (Fig. 3f) also blunted NA-stimulated respiration in $Ckb^{fl/fl}$ control, but not $Ckb^{AdipoqCre}$ brown adipocytes (Fig. 3g, h) with no impact on basal respiration (Extended Data Fig. 7c). Together, these data suggest that both CKB and a_1AR signaling are essential components of NA-stimulated thermogenesis.

Coordinated Ga_q and Ga_s signaling promotes energy expenditure *through* CKB *in vivo*

Although our data, in addition to the work of others[32,33] independently suggested a key role of aAR signaling in adipocyte thermogenesis, the precise G protein class that couples aAR activation to signaling in the interior of brown adipocytes has never been defined. Thus, we first examined the G protein coupling profile of a_{1A}AR by measuring agonist-induced BRET between ADRA1A-tagged Nano Luciferase (ADRA1A-Nluc) and Venus-tagged miniG protein probes in immortalized brown adipocytes (Fig. 4a). Upon agonist stimulation by the a_{1A}AR selective ligand A61603, the a_1AR agonist cirazoline, or NA, ADRA1A-Nluc rapidly and primarily coupled to Ga_q (Fig. 4b), partially to Ga_s and Ga_i (Extended Data Fig. 8a, b), and minimally to Ga_o or Ga_{12} (Extended Data Fig. 8c, d). Next, to determine if aAR signaling regulates energy

expenditure *in vivo*, we employed a chemogenetic approach using DREADDs (designer receptors exclusively activated by designer drugs)[34,35]. As ADRA1A is primarily coupled to Ga_q in brown adipocytes (Fig. 4b), we constructed mice that conditionally express a HA-tagged modified muscarinic receptor (HA-hM3Dq) selectively in adipocytes (*hM3Dq*^{AdipoqCre}) (Fig. 4c, d). Fat-selective hM3Dq expression renders these mice capable of activating Ga_q signaling upon binding the inert molecule deschloroclozapine (DCZ)[36]. Then, to determine if Ga_q signaling functions through *Ckb*, we crossed *hM3Dq*^{AdipoqCre} mice to *Ckb*$^{fl/fl}$ mice to construct mice where Ga_q signaling could be activated selectively in *Ckb*-expressing (*hM3Dq*^{AdipoqCre}:*Ckb*$^{fl/+}$) or *Ckb*-deficient (*hM3Dq*^{AdipoqCre}:*Ckb*$^{fl/fl}$) adipocytes. All mice were single-housed at 30ºC and injected i.p. with either CL 316,243 (to activate Ga_s through b_3AR stimulation) or DCZ + CL 316,243 (to activate both Ga_q and Ga_s through hM3Dq and b_3AR stimulation, respectively) (Fig. 4e). In both *hM3Dq*^{AdipoqCre}:*Ckb*$^{fl/+}$ and *hM3Dq*^{AdipoqCre}:*Ckb*$^{fl/fl}$ mice, saline treatment caused a transient spike in energy expenditure that rapidly subsided within one hour (Fig. 4f, g). Notably, combined treatment of *hM3Dq*^{AdipoqCre}:*Ckb*$^{fl/+}$ mice with DCZ and CL 316,243 elevated sustained energy expenditure to a significantly higher (by about 30%) level compared to CL 316,243 treatment alone (Fig 4h). In contrast, adipocyte-selective loss of *Ckb* impeded the capacity for combined DCZ and CL 316,243 treatment to stimulate whole body energy expenditure above CL 316,243 (Fig. 4i). DCZ was not sufficient on its own to trigger sustained energy expenditure (Extended Data Fig. 9a), further indicating that acute activation of Ga_q signaling needs to be superimposed on Ga_s activation to influence energy expenditure. Collectively, these data imply that *Ckb* is genetically required for the stimulation of adipocyte energy expenditure through combined Ga_s and Ga_q activation *in vivo*.

Overlaying a_{1A}AR activation on cAMP signaling promotes CKB-dependent thermogenesis

Ga_q and Ga_s signaling are engaged in all adipose depots (white and brown) of *hM3Dq*^{AdipoqCre} mice treated with DCZ and CL 316,243. Thus, we next probed the sufficiency of a_1AR signaling to enhance cAMP-stimulated brown adipocyte-intrinsic thermogenesis and whether CKB is required for this effect (Fig. 4j). Mimicking bAR signaling (by augmenting intracellular cAMP levels through direct stimulation of adenylyl cyclase with forskolin) did not match the respiratory response achieved with NA in *Ckb*$^{fl/fl}$ brown adipocytes (Fig. 4k, l). We confirmed that the maximal rate of forskolin-stimulated respiration had been reached because doubling the forskolin concentration did not further elevate respiration (Extended Data Fig. 9b). Similar to individual application of DCZ, a_1AR agonism (cirazoline) was not sufficient on its own to stimulate oxygen consumption (Fig. 4k, l). Thus, separately elevating either cAMP levels or engaging a_1AR signaling does not recapitulate NA-stimulated thermogenesis. Notably, combined treatment with forskolin and cirazoline elicited a thermogenic response similar to NA in *Ckb*$^{fl/fl}$ brown adipocytes (Fig. 4k, l), whereas the a_1AR-mediated component of respiration was blocked (by 90%) in *Ckb*^{AdipoqCre} compared to *Ckb*$^{fl/fl}$ brown adipocytes (Fig. 4k, l). Next, we tested the sufficiency of selective a_{1A}AR agonism (A61603) to induce respiration cooperatively with cAMP (Fig. 4m). When combined with cAMP signaling, A61603 induced respiration in control *Ckb*$^{fl/fl}$ brown adipocytes to the

same level achieved with NA; however, this response was significantly impaired (by about 80%) in *Ckb*^{AdipoqCre} brown adipocytes (Fig. 4n, o). Together, these data demonstrate that the coordinated activation of a_{1A}AR and cAMP signaling converges upon CKB to promote thermogenesis by brown adipocytes.

Discussion

NA is understood to be the predominant physiological regulator of ligand-mediated adaptive and facultative adipocyte thermogenesis[1]. bAR signaling and Ga_s-coupled cAMP production has dominated the focus of sympathetic activation of BAT, leaving the aAR-dependent component a relatively under-explored area of adipocyte biology. A role for aAR signaling in adipocyte thermogenesis has been demonstrated previously[33,37,38]; however, the particular aAR sub-type, the class of G protein that its coupled to, and the effector protein(s) that transduce aAR signaling into a thermogenic output have all remained elusive.

In thermogenic fat, creatine liberates a molar excess of mitochondrial ADP to promote thermogenic respiration through a futile creatine cycle catalyzed by CKB and TNAP[3,4]. However, the signal transduction pathways and transcriptional regulators that orchestrate futile creatine cycling gene expression with acute regulation of thermogenesis have remained mysterious. In this study we uncover that when combined with cAMP tone, activation of the a_{1A}AR subtype signals through Ga_q to further enhance thermogenesis in brown adipocytes. Since CKB is necessary for thermogenesis by the futile creatine cycle, we used *Ckb* loss-of-function models to explore the role of the futile creatine cycle in a_{1A}AR-stimulated thermogenesis. We reveal CKB as a necessary effector for nearly all of the a_{1A}AR-stimulated thermogenic component. The following data support this conclusion: First, NA-stimulated thermogenesis is significantly reduced in *Ckb*^{AdipoqCre} compared to *Ckb*$^{fl/fl}$ brown adipocytes. Second, antagonism of aAR or a_1AR signaling in *Ckb*$^{fl/fl}$ brown adipocytes decreases NA-dependent respiration to the same lower level elicited by *Ckb*^{AdipoqCre} brown adipocytes, while aAR or a_1AR antagonism has no effect on NA-stimulated respiration of *Ckb*^{AdipoqCre} brown adipocytes. Third, superimposing a_1AR or a_{1A}AR activation on cAMP signaling elicits thermogenesis akin to NA only in control *Ckb*$^{fl/fl}$ brown adipocytes but not *Ckb*^{AdipoqCre} brown adipocytes. Fourth, CKB is necessary for fat-selective Ga_q signaling to enhance whole-body energy expenditure above b_3AR-stimulated thermogenesis. In addition to defining the features of acute thermogenic activation by combined a_{1A}AR and cAMP signaling, we delineate the transcriptional control of futile creatine cycling genes to be similarly orchestrated by mutual a_1AR and b_3AR signaling via EBF1/2, ERRa/g, and PGC1a.

The a_1AR family contains three subtypes (a_{1A}, a_{1B}, and a_{1D}), which are all engaged by NA[39]. We demonstrate that the a_{1A} subtype (*Adra1a*) is the most abundant in brown adipocytes, but a_{1D} (*Adra1d*) is also expressed. Addressing this complexity using fat-selective knockout mouse models, possibly even double knockouts (*Adra1a* and *Adra1d*), will be a key area of future research to genetically uncover the

required role of individual a_1AR subtypes in brown fat thermogenesis *in vivo*. Until then, a complete understanding of the signal transduction cascade that couples ligand-mediated a_1AR activation with thermogenesis by the futile creatine cycle remains to be determined.

Chronic Ga_q activation has been reported to inhibit adipocyte differentiation and thermogenic output[40]. In marked contrast, we reveal a key role for Ga_q signaling in promoting thermogenesis. These distinct results may be due to our focus on the acute (as opposed to chronic) Ga_q activation of thermogenesis through the futile creatine cycle (as opposed to UCP1).

BAT is associated with cardiometabolic benefits[41-44]. However, given the variability of existing BAT depots in humans, along with the reductions of BAT activity in obesity, a full understanding of the molecular mechanisms that promote the greatest activation of adipocyte thermogenesis is of considerable interest to uncover if BAT is a viable clinical target that can enhance cardiometabolic health[45-49]. Clinical relevance of aAR-triggered BAT thermogenesis is exemplified by conditions such as hypothyroidism, where aAR signaling may contribute more towards thermogenic respiration than bAR signaling[50], and in the context of NA-secreting paragangliomas, where aAR blockade reduces both glucose uptake by adipose tissue and whole body energy expenditure[32].

Ckb is expressed in *Ucp1*$^+$ adipocytes[3], as is *Alpl*[4], and we demonstrate that loss of *Ckb* decreases NA-stimulated thermogenesis even in the presence of UCP1. Thus, our data imply that multiple metabolic heat generating pathways co-exist in BAT. Discrete thermogenic pathways could segregate inter- or intra-cellularly. The identification of distinct adipocyte subtypes[51-56] as well as mitochondrial heterogeneity within thermogenic fat cells[57] supports this idea. Thus, the futile creatine cycle probably operates in conjunction with UCP1-dependent thermogenesis. Of course, the fractional proportion of these two pathways will be dynamic and depend on extrinsic stimuli, regulated by important factors such as thermal history. Whether other thermogenic pathways also similarly operate in parallel with the futile creatine cycle and UCP1 in adipocytes remains to be determined.

Methods

Animals

Mouse experiments were performed according to procedures approved by the Animal Resource Centre at McGill University and complied with guidelines set by the Canadian Council of Animal Care. The photoperiod was fixed at 12 hour:12 hour with lights on at 0700 hours (Zeitbeger time 0, ZT0). Mice had *ad libitum* access to drinking water and a low fat diet (3.1 kcal/g energy density) with 24%, 16%, and 60% of Calories from protein, fat, and carbohydrate, respectively (2920X, Envigo, Madison, WI, USA). All mice were born and housed in groups (3-5 mice per cage) at 22°C with bedding and shredded paper strips in the cage until experimental intervention. Wild-type C57BL/6N mice were purchased from Charles River (strain code: 027). *Ckb*$^{fl/fl}$ mice were previously described[3]. Ucp1CreERT2 mice[58] were bred to

Ppargc1a$^{fl/fl}$ mice to generate experimental groups (*Ppargc1a*$^{fl/fl}$ and *Ppargc1a*^{Ucp1CreERT2}). AdipoqCre mice (B6;FVB-Tg(AdipoQ-Cre)1Evdr/J), stock 028020), maintained on a C57BL/6J background, were bred to (*Ckb*$^{fl/f}$)[l3], (*Ebf1/2*$^{fl/fl}$)[26], and (*Esrra/g*$^{fl/fl}$)[27,59,60] mice to generate experimental groups (*Ebf1/2*$^{fl/fl}$ and *Ebf1/2*^{AdipoqCre})[26] (*Esrra/g*$^{fl/fl}$ and *Esrra/g*^{AdipoqCre}) (*Ckb*$^{fl/fl}$ and *Ckb*^{AdipoqCre}). LSL-hM3Dq-DREADD mice (B6N;129-Tg(CAG-CHRM3*,-mCitrine)1Ute/J), stock 026220) were bred to AdipoqCre mice to generate mice that conditionally express a HA-tagged modified muscarinic receptor (HA-hM3Dq) selectively in adipocytes (*hM3Dq*^{AdipoqCre}). *hM3Dq*^{AdipoqCre} mice were crossed with *Ckb*$^{fl/fl}$ mice to generate *hM3Dq*^{AdipoqCre}:*Ckb*$^{fl/+}$ or *hM3Dq*^{AdipoqCre}:*Ckb*$^{fl/fl}$ mice. Mouse experiments used age-matched littermates and were conducted at the temperature indicated in each figure legend. For cold exposure experiments, mice were singly housed in cages with bedding and shredded paper strips and with *ad libitum* access to drinking water and a low fat diet.

Inducible deletion of *Ppargc1a*

Mice were reared at 21°C-22°C until 7 weeks of age, then injected with tamoxifen (75 mg kg−1) for 3 days and allowed to recover for 4 days until intervention.

Genotyping

Ckb (WT and conditional alleles): Ckb forward, 5'-AGG TGG TGG CTA GAG TGA GC-3'; *Ckb* reverse, 5'-CAA GGA TCC CAC TGC TCT TC-3'.

Adrb1: Adrb1^{+} forward, 5'-TCG CTA CCA GAG TTT GCT GA-3'; *Adrb1*$^{+}$ reverse, 5'-GGC ACG TAG AAG GAG ACG AC-3'. *Adrb1*$^{-}$ forward, 5'-TCG CCT TCT TGA CGA GTT CT-3'; *Adrb1*$^{-}$ reverse, 5'-TGG CTC TCT ACA CCT TGG AC-3'.

Ebf1/Ebf2 (WT and conditional alleles): Ebf1 forward, 5'-CCC CCA CTT CTT GAG GCC TGT GTT GC-3'; *Ebf1* reverse, 5'-CCT GGG AGT GGA GGG AGG AAG GAA AAT-3'. *Ebf2* forward, 5'-GAA CTT GGG GCC AGC CTT TT-3'; *Ebf2* reverse, 5'-TGT CCT TGA GCT CCC AGG CT-3'.

Essra/Essrg (WT and conditional alleles): Essra forward, 5'-ATG AGC CAG GAT GCA GGT GCC TGC A-3'; *Essra* reverse, 5'-GGC TGA GGC AAA GGG ATG GAG GGG T-3'. *Essrg* forward, 5'-GTT TTA AAG GCC CTT GGT GAT CTC GC-3'; *Essrg* reverse, 5'-CTGCAACCCTTGGACTGCCAGAAC-3'.

Ppargc1a (WT and conditional alleles): Ppargc1a forward, 5'-TCC AGT AGG CAG AGA TTT ATG AC-3'; *Ppargc1a* reverse, 5'-TGT CTG GTT TGA CAA TCT GCT AGG TC-3'.

CAG-LSL-Gq-DREAD: GqDREADD forward, 5'-CGC CAC CAT GTA CCC ATA C-3'; GqDREADD reverse, 5'-GTG GTA CCG TCT GGA GAG GA-3'.

AdipoqCre: AdipoqCre forward, 5'-ACG GAC AGA AGC ATT TTC CA-3'; AdipoqCre reverse, 5'-GGA TGT GCC ATG TGA GTC TG-3'.

Ucp1CreERT2: Ucp1CreERT2 forward, 5'-GAA CCT GAT GGA CAT GTT CAG G-3'; Ucp1CreERT2 reverse, 5'-AGT GCG TTC GAA CGC TAG AGC CTG T-3'.

ERRα ChIP-qPCR

For each condition, nuclei were isolated from 6 individual BAT pads from 3 male wild-type (C57Bl6/N) mice. BAT was dounce homogenized (25 times with pestle A and 15 times with pestle B) in Nuclei Preparation Buffer (10 mM HEPES pH 7.5, 10 mM KCl, 1.5 mM $MgCl_2$, 0.1% NP40). BAT homogenate was filtered through 100mm strainer. Nuclei were fixed with 1% formaldehyde for 12 minutes at room temperature, quenched by 125 mM of glycine for 10 minutes and washed twice with 0.1% NP40 in PBS. Chromatin was sonicated in 1 ml of Sonication buffer (50 mM Tris-Hcl pH 8.1, 10 mM EDTA, 1% SDS) to obtain fragments around 500 bp. 20 µg of chromatin DNA was diluted in ChIP Dilution Buffer (16.7 mM Tris-HCl pH8.1, 1.1% Triton X-100, 167 mM NaCl, 1.2 mM EDTA, 0.01% SDS) up to 2 ml. 0.87 µg of anti-ERRα antibody (Abcam, ab76228) was added to the sonicated chromatin and left to rotate overnight at 4ºC. The next day, 50 µl of Dynabeads™ Protein G (Cat. No. 10009D, Thermo Fisher Scientific) were washed twice with PBS+0.5% TWEEN, 0.5% BSA and added to the chromatin for 1 hour under rotation at 4ºC. Next, Dynabeads were washed 2 times with 1 ml of cold Low Salt RIPA Buffer (0.1% SDS, 1% Triton x-100, 1 mM EDTA, 20 mM Tris-HCl pH 8.1, 140 mM NaCl, 0.1% Na-deoxycholate), 2 times with 1 ml of cold High Salt RIPA Buffer (0.1% SDS, 1% Triton x-100, 1 mM EDTA, 20 mM Tris-HCl pH 8.1, 500 mM NaCl, 0.1% Na-deoxycholate), 2 times with 1 ml of cold LiCl Wash Buffer (250 mM LiCl, 0.5% NP40, 0.5% Na deoxycholate, 1 mM EDTA,10 mM Tris-HCl pH 8.1) and 2 times with room temperature TE buffer (10 mM Tris-HCl pH8.0, 1 mM EDTA pH 8.0). DNA was eluted overnight at 65ºC with 100 µl of ChIP Elution Buffer (10 mM Tris-HCl pH 8.0, 5 mM EDTA, 300 mM NaCl, 0.1% SDS, 5 mM DTT) and 16 µl Reverse Cross-Linking mix (250 mM Tris-HCl pH 6.5, 62.5 mM EDTA pH 8.0, 1.25 M NaCl, 5mg/ml Proteinase K, 62.5µg/ml RNase A). Finally, immunoprecipitated chromatin DNA was purified using a QIAquick PCR purification kit and eluted in 31 µl of Elution buffer (10 mM Tris-HCl pH8.0, 0.1 mM EDTA pH8.0). Relative ChIP fold enrichments were controlled by inputs and normalized to the average of 2 non-specific control regions using a LightCycler 480 (Roche) using SYBR Green I Master Mix (Cat. No. 4887352001, Roche) as previously published[61]. Results represent the average of 3 replicates. Gene-specific and non-specific control primers used for ChIP-qPCR analysis are as follows: *ERRα -550 (positive control)* (forward, GTG GCC CCG CCT TTC CCC GTG ACC TTC ATT; reverse, ACC CCT GAG GAC CCT CAA GTG GAG AAG CAG); *ERRα -3722 (negative control)* (forward, TTG GCA TTG ATA TTG GGG GTG GGA GCA ACT; reverse, GAC TTC TTA CTT TGA CGC TTT CCT CCA TCG); *Prox1 -55772 (negative control)* (forward, CCA AGC ACA AAT ATC TAA TCA CCC TTT C; reverse, CTT CTT GAT AGG TTT ATG GGT TGG GC); *Ckb DAR 1* (forward, GAC CTG CAA ACC ACT TGG GAC C; reverse, GAT GCG CTG GAC TCT GAC GAT G); *Ckb DAR 2* (forward, CAG ACG CCA AAG AGA CTG GTC A; reverse, CCT AGT TTG TGC AGT GCC TCC C); *Alpl DAR 1* (forward, CAC TGG CCC CAT ACT TCA GGG T; reverse, AGG CTT CTC AGC TCT TGG GGA G); *Alpl DAR 2* (forward, GGG CAG AAG GCT TGT CCA AGG G; reverse, GAG CTG ACA TGT CCA GAA AAG AGC); *Alpl DAR 3* (forward, TTC TTC TCA CAA GCC CCA GGC; reverse, AGG CTC CCC GGT GAC CTT TTA G); *Alpl DAR 4* (forward, GGC TGC CAG AGC TGG AAA TCA G; reverse, AAC CCA TGA GGC TGT CTG GTG T); *Alpl DAR 5* (forward,

GTC ACT GAC CCA GCA ACT ATA GCC; reverse, TCT AGG GTC AAT ATC CTG CCC A); *Alpl DAR 6* (forward, TTG CTG TCC CAT CTG TAC CTG A; reverse, TGG TGA CCT CTT AAC AAC AGA GTG GC); *Alpl DAR 7* (forward, AGG CCA CTC ACC TCT GCA GTC; reverse, GGA GGG TGG AGC TAG GGG TGA T); *Alpl DAR 8* (forward, TCC CCT CCC TTT TGC TTT GTT TC; reverse, GCA TTT CAA GGT GGC AGC CAG A).

Administration of chemicals by osmotic pump

Osmotic pumps (Alzet) were loaded with CL 316,243 in 100 µl total volume. Mice were anesthetized with isoflurane. A small skin incision was made directly above the interscapular BAT depot. Filled osmotic pumps were placed above the interscapular BAT and the skin was then sewed. Tissues were harvested for gene expression analyses following intervention. The release rate from the osmotic pumps is 0.5 µl per hour, so, as an example, loading 0.5mg of CL 316,243 in 100 µl for a 24g mouse will administer approximately 0.1mg kg^{-1} CL 316,243 every hour.

Administration of chemicals by intraperitoneal injection

Phenoxybenzamine (PBZ) was dissolved in saline and was injected (5mg kg^{-1}) once over 24 hours. Prazosin (PZS) was dissolved in 4% DMSO, 30% PEG, 66% saline and was injected (5mg kg^{-1}) three times over 24 hours. Propranolol hydrochloride (PBZ) was dissolved in saline and was injected (5mg kg^{-1} or 10mg kg^{-1}) 1 hour prior to cold exposure and then two additional time (three times total) over 24 hours.

RNA extraction

Total RNA from frozen mouse tissues was extracted using QIAzol (Qiagen) and purified with RNeasy Mini spin columns (Qiagen) according to the manufacturer's instructions. Total RNA from human tissues, third cohort, was extracted with TRIzol (Gibco BRL, Life Technologies, Roskilde, Denmark). RNA was quantified using a NanoDrop 8000 Spectrophotometer (Thermo Scientific Pierce, Waltham, Maine, USA). cDNA was synthesized using a Verso cDNA kit (cat# Ab-1453, Thermo Fischer Scientific) with random hexamer primers.

Reverse transcription quantitative polymerase chain reaction (RT-qPCR)

Purified RNA was reverse-transcribed using a High-Capacity cDNA Reverse Transcription kit (Applied Biosystems). The resultant cDNA was analysed by RT-qPCR. In brief, 20 ng cDNA and 150 nmol of each primer were mixed with GoTaq qPCR Master Mix (Promega). Reactions were performed in a 384-well format using a CFX384 Real-time PCR system (Bio-rad). Normalized mRNA expression was calculated using the ΔΔCt method, using *Ppib* or *36b4* mRNA as the reference gene. CFX Maestro 2017 was used for data collection. Primer sequences used for RT–qPCR of mouse samples are as follows: *Ckb* (forward, GCC TCA CTC AGA TCG AAA CTC; reverse, GGC ATG TGA GGA TGT AGC CC); *Alpl* (forward, CCA ACT CTT TTG TGC CAG AGA; reverse, GGC TAC ATT GGT GTT GAG CTT TT); *Ppargc1a* (forward, AGC CGT GAC CAC TGA CAA CGA G; reverse, GCT GCA TGG TTC TGA GTG CTA AG); *Esrra* (forward, CCA GAG GTG GAC CCT TTG CCT TTC; reverse, CAC CAG CAG ATG CGA CAC CAG AG); *Esrrg* (forward, CTC CAG CAC CAT

CGT AGA GGA TC; reverse, GAT CTC ACA TTC ATT CGT GGC TG); *Ucp1* (forward, AAG CTG TGC GAT GTC CAT GT; reverse, AAG CCA CAA ACC CTT TGA AAA); *Ebf1* (forward, CCA ACA GCG AAA AGA CCA ATA A; reverse, TGT TCT GTC CGT ATC CCA TTG); *Ebf2* (forward, CCA GCT CTG AAA GAC AAG TCG; reverse, GAG GTT GCT TTT CAA AAT GGG C); *Ppib* (forward, GGA GAT GGC ACA GGA GGA A; reverse, GCC CGT AGT GCT TCA GCT T); *Rps18* (forward, CAT GCA GAA CCC ACG ACA GTA; reverse, CCT CAC GCA GCT TGT TGT CTA), *36b4* (forward, TCA TCC AGC AGG TGT TTG ACA; reverse, GGC ACC GAG GCA ACA GTT). For human samples, PCR reactions were performed in duplicate using LightCycler SYBR Green master mix (Roche Applied Science) in a LightCycler 480 (Roche Applied Science). The following cycling conditions were used: One step at 95 °C for 3 min, then 95°C for 10 seconds, 60°C for 20 seconds and 72°C for 10 seconds, and finally a melting curve analysis was performed. The increase in fluorescence was measured in real time during the extension step. The relative gene expression was estimated using the default “Advanced Relative Quantification” mode of the software version LCS 480 1.5.1.62 (Roche Applied Science) and specificity of the amplification was checked by melting curve analysis. Normalized mRNA expression for human samples was calculated using *PPIA* as the reference gene. Primer sequences used for RT–qPCR of human samples are as follows: *CKB* (forward, ACT TCA GAA GCG AGG CAC AG; reverse, GAT GAG CAG CTT CAC TCC GT); *ADRA1A* (forward, AAT GCT TCC GAC AGC TCC AA; reverse, TAG TGC GTG ACT GAG TGC AG); *PPIA* (forward, TCC TGG CAT CTT GTC CAT; reverse, TGC TGG TCT TGC CAT TCC T).

RNA sequencing analysis

Total RNA was quantified using a NanoDrop Spectrophotometer ND-1000 (NanoDrop Technologies, Inc.) and its integrity was assessed on a 2100 Bioanalyzer (Agilent Technologies). Libraries were generated from 250 ng of total RNA as following: mRNA enrichment was performed using the NEBNext Poly(A) Magnetic Isolation Module (New England BioLabs). cDNA synthesis was achieved with the NEBNext RNA First Strand Synthesis and NEBNext Ultra Directional RNA Second Strand Synthesis Modules (New England BioLabs). The remaining steps of library preparation were done using and the NEBNext Ultra II DNA Library Prep Kit for Illumina (New England BioLabs). Adapters and PCR primers were purchased from New England BioLabs. Libraries were quantified using the Kapa Illumina GA with Revised Primers-SYBR Fast Universal kit (Kapa Biosystems). Average size fragment was determined using a LabChip GX (PerkinElmer) instrument. The libraries were normalized and pooled and then denatured in 0.05N NaOH and neutralized using HT1 buffer. The pool was loaded at 225pM on a Illumina NovaSeq S4 lane using Xp protocol as per the manufacturer’s recommendations. The run was performed for 2x100 cycles (paired-end mode). A phiX library was used as a control and mixed with libraries at 1% level. Base calling was performed with RTA v3.4.4 . Program bcl2fastq2 v2.20 was then used to demultiplex samples and generate fastq reads. Adaptor sequences and low quality score bases (Phred score < 30) were first trimmed using *Trimmomatic v.0.36*[62]. The resulting reads were aligned to the GRCm38 mouse reference genome assembly, using *STAR v.2.0.2*[63]. Read counts were obtained using *HTSeq v.0.6.0*[64] with parameters *-m intersection-nonempty -stranded=reverse*. For all downstream analyses, we excluded lowly-expressed genes with an average read count lower than 10 across all samples, resulting in 17,952 genes

in total. Raw counts were normalized using *edgeR*'s TMM algorithm *v3.26.8*[65] and were then transformed to log2-counts per million (logCPM) using the *voom* function implemented in the *limma* R package[66]. To assess differences in gene expression levels between the different conditions, we fitted a linear model using *limma*'s *lmfit* function. Nominal p-values were corrected for multiple testing using the Benjamini-Hochberg method. To specifically identify temperature-sensitive genes that further respond differently to PBZ treatment, we first obtained differentially expressed genes in 6°C vs 6°C+PBZ (FDR < 0.1) and then filtered for those that change expression in comparison to 30°C (i.e., in either 6°C vs 30°C or 6°C+PBZ vs 30°C; FDR < 0.01 and |log2FC| > 1). Unsupervised hierarchical clustering of the 764 differentially expressed genes showed four distinct patterns of changes in expression (R *hclust* function). The complete list of differentially expressed genes and their cluster annotation is presented in Extended Data Table 1. Enrichment analysis of Gene Ontology (GO) Biological Processes were performed using Enrichr[67]. The enrichment results for cluster 4 are reported in Extended Data Fig. 1i.

Generation of ATAC sequencing libraries from BAT

For each condition, nuclei were isolated from 4 individual frozen BAT pads from 2 male wild-type (C57Bl6/N) mice. Animals were housed at 30°C for 5 days then exposed to cold (6°C) or kept at 30°C for 24 hours. Mice were injected with vehicle (0.9% saline) or phenoxybenzamine (5 mg kg^{-1}) 1 hour prior to cold exposure. Our protocol and the buffers used were adapted from[68] with some modifications. Briefly, for nuclei preparation, BAT pads were homogenized (with pestle A) in a pre-chilled 2 ml Dounce homogenizer containing 2 ml cold 1x Homogenization Buffer (60 mM Tris pH 7.8, 30 mM $CaCl_2$, 18 mM $MgAc_2$, 320 mM sucrose, 0.1 mM EDTA, 0.1% NP40, 0.1mM PMSF, 1mM b-mercaptoethanol). The resulting solution was pre-cleared using a 100 µm filter and grounded 20 times (with pestle B). To generate the iodixanol gradient, 1 volume (800 µl) of 50% Iodixanol solution was added to 800 µl of grounded BAT solution to give a final concentration of 25% Iodixanol in a 5 ml Low-Bind Eppendorf tube. Then, 1.2 ml of 29% Iodixanol solution was added under the 25% mixture, and another 1.2 ml of 35% Iodixanol solution wad added under the 29% mixture. The gradient was centrifuged 3,000 g for 20 minutes at 4°C with the brake off. The nuclei band was collected into a new tube and nuclei were counted using trypan blue staining and Countess® II FL automated cell counter. 50,000 nuclei were transferred into a tube containing 1 ml of ATAC-RSB+0.1% Tween-20 and centrifuged 500 g for 10 minutes at 4°C. For optimized transposition, Omni-ATAC ATAC-seq reaction mix (25 µl 2x TD buffer, 100 nM transposase, 16.5 µl PBS, 0.01% digitonin, 0.1% Tween-20)[68] was added to the nuclei pellet. Nuclei were resuspended by pipetting up and down 6 times. The resulting solution was incubated at 37°C for 30 minutes in a thermomixer (1,000 RPM). For the pre-amplification of transposed fragments, solution was cleaned with a Zymo DNA Clean and Concentrator-5 kit (Cat. No. D4014) according to the manufacturer's instructions. DNA was eluted in a 21 µl elution buffer and amplified for 5 cycles using NEBNext 2x MasterMix (NEB, M0541L) as previously described (PMID: 28846090), using published primers (PMID: 24097267). 10% of the pre-amplified mixture, was used to run a qPCR to determine the number of additional cycles needed as previously described[68]. Next, the amplification profiles were manually assessed and the required number of additional cycles were determined as previously described[69]. The

final PCR reaction was purified using a Qiagen MinElute PCR Purification Kit and eluted in 20 µl elution buffer. A subsample of each library was diluted to 1:1,000 to fall within range of the standards to perform concentration quantification using the KAPA Library Quantification Kit (Cat No. KK4854) according to the manufacturer's instructions. Paired end, 150 bp sequencing was performed on a HiSeq instrument at the Michael Smith Genome Sciences Centre (BC Cancer Research Institute).

ATAC sequencing analysis

ATAC-seq reads were first trimmed for adapter sequences and low quality score bases using Trimmomatic[62]. The resulting reads were mapped to the mouse reference genome (mm10) using BWA-MEM[70] in paired-end mode at default parameters. Only reads that had a unique alignment (mapping quality > 20) were retained and PCR duplicates were marked using Picard tools (https://broadinstitute.github.io/picard/). Peaks were called and annotated using MACS2[71]. Peak annotation and transcription factor (TF) motif enrichment analysis were performed using the *annotatePeaks* and *findMotifsGenome* commands, respectively, from HOMER software suite[72]. Peaks were associated to a gene if located within 20 kb of the TSS. To assess differences in chromatin accessibility, a "reference peak set" was generated by merging ATAC-seq peaks across samples, using *bedtools merge* with parameters: *-sorted -d -125* (https://bedtools.readthedocs.io/). Read counts were obtained within these genomic regions using HOMER. Raw counts were normalized using edgeR's TMM algorithm[65] and were then transformed to log2-counts per million (logCPM) using the *voom* function implemented in the *limma* R package[66]. To test for differential occupancy, we fitted a linear model that takes into account the batch effects in the experiment. Nominal p-values were corrected for multiple testing using the Benjamini-Hochberg method. Read density metagene plots and heatmaps were obtained using ngs.plot[73] with the following parameters: *-G mm10 -BOX 0 -SE 0 -VLN 0 -LWD 2 -WD 9 -L 1500*. Genome browser tracks were created with the HOMER *makeUCSCfile* command and *bedGraphToBigWig* utility from UCSC. Tracks were normalized so that each value represents the read count per base pair per 10 million reads. UCSC Genome Browser (http://genome.ucsc.edu/) was implemented for track visualization.

Western blotting

Samples were prepared in lysis buffer (50 mM Tris, pH 7.4, 500 mM NaCl, 1% NP40, 20% glycerol, 5 mM EDTA and 1 mM phenylmethylsulphonyl fluoride (PMSF)), supplemented with a cocktail of Roche protease inhibitors. The homogenates were centrifuged at 16,000g for 10 min at 4°C, and the supernatants were used for subsequent analyses. Protein concentration was determined using the bicinchoninic acid assay (Pierce). The quantity of protein lysate to use for each antibody was determined empirically. Protein lysates were denatured in Laemmli buffer (60 mM Tris, pH 6.8, 2% SDS, 10% glycerol, 0.05% bromophenol blue, 0.7 M β-mercaptoethanol), resolved by 10% Tris/Glycine SDS–PAGE and transferred to a polyvinylidene difluoride (PVDF) membrane. Primary antibodies were diluted in TBS containing 0.05% Tween (TBS-T), 5% BSA and 0.02% NaN3. Membranes were incubated overnight with primary antibodies at 4ºC. For secondary-antibody incubation, anti-rabbit or anti-mouse HRP (Promega)

was diluted at 1:10,000 (v/v) in TBS-T containing 5% milk. Results were visualized with enhanced chemiluminescence Western blotting substrates (Bio-Rad). Dilutions for antibodies were as follows: vinculin (VCL) (Cell Signaling; cat. no. 13901; clone E1E9V; dilution: 1:5,000); CKB (Abclonal; cat. no. ab12631; 1:1,000); UCP1 (Abcam; cat. no. ab10983; dilution: 1:2,000); TNAP (R&D; cat. no. AF2910; 1:200); ERRa (Abcam; cat. no. ab76228; 1:1,000); GFP (Abclonal; cat. no. ab290; 1:1,000); HA-Tag (Cell Signaling; cat. no. C29F4; 1:1,000); Anti-rabbit (Promega; cat. no. W401B; dilution: 1:10,000); Anti-mouse (Promega; cat. no. W402B; dilution: 1:10,000); Anti-goat (Promega; cat. no. V805A; dilution: 1:10,000).

Indirect calorimetry

Mice had *ad libitum* access to drinking water and a low fat diet (2920X, Envigo). All mice used for indirect calorimetry experiments were born and housed in groups (3-5 mice per cage) at 22°C with bedding and shredded paper strips in the cage until experimental intervention. Mice (6-8 weeks of age) were placed, single-housed, in metabolic cages (Sable Systems International, Promethion high-definition behavioural phenotyping system) housed in thermal cabinets set to 30°C with a 12-h light/dark schedule. Mice had *ad libitum* access to food and water and were allowed to acclimate to 30°C for 5 days. The following morning between Zeitgeber time (ZT) ZT2-3, mice were injected with vehicle (saline) and placed back in the metabolic cages to monitor the stress response to i.p. injection. The next morning (at ZT2-3), the same volume of the β_3-adrenoreceptor agonist CL 316,243 (0.5 mg kg^{-1}) or CL 316,243 + DCZ (0.5 mg kg^{-1} each) was administered i.p. and mice were placed back in the metabolic cages. For NA experiments, NA (Sigma, Cat. No. A9512) was prepared fresh in saline and administered i.p. at 1 mg kg^{-1} at 30°C. Responses to drugs were followed every 3 min. Mass-dependent variables (energy expenditure) was not normalized to body weight. Energy expenditure (kcal), physical movement (measured by infrared beam breaks), and food intake were recorded every 3 min using Sable Systems data acquisition software (IM-3 v.20.0.3). Data were analyzed using Sable Systems International MacroInterpreter software (v.2.41) using One-Click Macro (v.2.37).

Isolation of brown adipocytes

Interscapular BAT was minced and digested in a Krebs-Ringer bicarbonate modified buffer (KRBMB: 135 mM NaCl; 5 mM KCl; 1 mM $CaCl_2$; 1 mM $MgCl_2$; 0.4 mM K_2HPO4; 25 mM $NaHCO_3$; 20 mM HEPES; 10 mM glucose; 4% fatty acid-free BSA), supplemented with 2 mg/ml collagenase B (Worthington) and 1 mg/ml soybean trypsin inhibitor (Worthington). Minced BAT from 10 mice was digested in 20 ml KRBMB digestion buffer with continuous shaking at 37ºC for 45 minutes. The tissue suspension was filtered through a 100 µm cell strainer. Brown adipocytes were allowed to float for 5 minutes at room temperature before and after spinning at 100 g for 5 minutes. Half of the infranatant was removed (~10 ml) with a 20 ml syringe/18G needle, followed by the removal of the stromal vascular fraction (SVF). Adipocytes were washed with 10 ml DMEM/F12 supplemented with 10% FBS and were allowed to float for 20 minutes at room temperature before spinning at 200 g for 5 minutes. Adipocytes were washed three times. After the final wash, the mature adipocytes present under the fat layer were transferred to a new tube. Cell number was approximated by counting nuclei. Briefly the number of cells was counted by mixing 0.16% trypan

blue diluted in nuclease lysis buffer (NLB: 250 mM Sucrose; 10 mM Hepes; 10 mM KCl; 1.5 mM $MgCl_2$; 0.1% IGEPAL) with cells diluted in NLB (1:4 ratio cells:NLB). The mixture was left at room temperature for 10 minutes before applying 10 µl to the hemocytometer.

Respirometry of purified adipocytes using an oxygen electrode

A Clark type electrode (Rank Bros) was used to measure the oxygen consumption of adipocytes. DMEM/F12 supplied with 10% FBS was added to the chamber and left to equilibrate with atmospheric oxygen. Approximately 300,000 cells were then added to the chamber, covered with a lid and continuously stirred. The initial rate of cellular respiration prior to the addition of a thermogenic activator was termed “basal respiration”. Thermogenic drugs were added to the continuously stirring cells via a Hamilton syringe (0.1 µM noradrenaline, 3 µM forskolin, 1 µM cirazoline, 1 µM A61603). For traces containing aAR inhibitors, phenoxybenzamine (1 µM) and prazosin (1 µM) were added to the respiration buffer prior to the addition of cells. The excess of oxygen consumed upon the addition of the drugs was subtracted from the basal respiration rate to account for the drug-dependent oxygen consumption. Rank Brothers Dual Digital model 20: Picolog 6 data logging software was used for data collection.

Unilateral denervation of interscapular BAT (iBAT)

Unilateral denervation was carried out as previously described[22,74]. Briefly, 22°C-housed mice were anesthetized by inhalation of isoflurane (2.5% for induction, 1.5% for maintenance) and the incision site was shaved and disinfected using first 0.5% chlorohexidine in 85% ethanol and then 70% ethanol. Prior to surgery, mice received local anesthesia (lidocaine, 1.4 mg kg^{-1}) and general analgesia (Rimadyl, 10 mg kg^{-1}). The iBAT was prepared by a midline incision of the skin in the interscapular region and the detachment of the iBAT from the underlaying muscle layer. The five nerve fibers innervating the right iBAT lobe were identified and cut (denervated) and the nerve fibers innervating the left iBAT lobe were identified and touched with forceps (sham). Following the procedure, the fat pads were rinsed with sterile isotonic saline and the incision was closed with suture. The mice were individually housed in clean cages at 22°C with access to a 37°C heating pad during the first 24 h post operation. Animals were monitored daily.

Glycerol release

Freshly isolated brown adipocytes ($1x10^6$ cells in 0.3ml) were incubated in DMEM/F-12 (Thermo Fisher Scientific) supplemented with 4% fatty-acid-free BSA and incubated with NA (0.1 µM) and/or PBZ (1 µM) for 1 hour at 37°C. Following incubation, released glycerol was separated from the adipocytes by spinning through a centrifugal filter (Millipore sigma, UFC30LG25) at 8,000 g x 30 seconds at room temperature. The glycerol content in the media was determined using free glycerol reagent (Sigma, F6428) and glycerol standard solution (Sigma, G7793) at an absorbance of 540 nm after incubating the sample and standards with free glycerol reagent for 15 min at room temperature in the dark.

Plasmids

Adra1a-Nluc was generated by amplifying the full-length sequence of *Nluc* (including linker) from *Gpr120-Nluc* (forward: 5'-GAG GAA GTC TCG GAA TTC GCC GCC ATG GTC TTC-3'; reverse: 5'-ACC CTT TTA CGC CAG AAT GCG TTC GCA CAG C-3') and fusing it in frame to untagged *Adra1a* by amplifying the vector encoding *Adra1a* without its stop codon through the use of PCR (forward: 5'-CAT TCT GGC GTA AAA GGG TGG GCG CGC CGA CC-3' and reverse: 5'-GAA TTC CGA GAC TTC CTC CCC GTT TTC ACC GAG-3') and Gibson assembly. *Adra1a-Nluc* was PCR-amplified (forward: 5'-GAT ACC GGA TCC GCG ACG ATG GTG CTT CTT TCT GAA-3' and reverse: 5'-TGC TTA CTC GAG TTA CGC CAG AAT GCG TTC-3') and subcloned into pcDNA3 via BamH1 and Xho1 restriction sites.

Bioluminescence resonance energy transfer (BRET)-based miniG subtype recruitment

Immortalized mouse brown preadipocytes were grown with DMEM with 10% fetal bovine serum and penicillin/streptomycin. Upon confluency, cells were differentiated with DMEM containing a differentiation cocktail of 20 nM insulin, 1 µM dexamethasone, 0.5 µM rosiglitazone, 1 nM T3 and 500 µM methyl isobutyl xanthine. After 2 days of differentiation, media was replaced with DMEM with 10% FBS containing 1 nM T3 and 20 nM insulin. The next day, the differentiated adipocytes were transfected using TransIT-X2 (Mirus) as per manufacture's protocol. Briefly, plasmid DNA encoding *Adra1a-NanoLuc*, as well as venus-tagged miniG protein subtypes (miniG$_i$, miniG$_s$, miniG$_q$, miniG$_{12}$, miniG$_o$, provided by Nevin Lambert, Augusta University, GA, USA) were added to a sterile tube containing OptiMEM & TransIT-X2. The TransIT-X2:DNA complexes were plated into selected wells of a 96-well white polystyrene Nunc microplate (Sigma) and left to incubate at room temperature for 15–30 minutes. Differentiated adipocytes were trypsinized and resuspended in DMEM with 10% fetal bovine serum and applied to selected wells at a density of 60,000 cells/well and incubated overnight.

For BRET experiments, 24-hours post-transfection, differentiated adipocyte media was replaced with Hank's balanced salt solution (HBSS) supplemented with 10 mM HEPES, pH 7.5, and 10 µM furimazine (NanoGlo, Promega). BRET measurements were performed at 37°C using a PHERAstar Microplate Reader (BMG Labtech) with a dual-luminescence readout BRET1 plus filter (donor wavelength: 460-490 nm band-pass, acceptor wavelength: 520-550 nm long-pass). Following four baseline measurements, the cells were treated with vehicle or agonists (NA, Cirazoline or A61603) in triplicate for each condition, with the BRET signal measured every 2 min for 1 h. The BRET ratio (acceptor 520-550nm emission over donor 460-490 nm emission) was calculated for each well over time. The resulting ligand-induced BRET ratio was calculated by subtracting the baseline vehicle read from the agonist-stimulated read for each condition.

Human studies

In this report, we have utilized human adipose tissue biopsies collected from two independent cohorts.

First cohort – Joslin Diabetes Center adipose tissue cohort: Details on procedures of human subject adipose tissue biopsy collection and clinical characteristics of subjects have been described previously[75,76]. Briefly, ten paired human neck fat samples were obtained from superficial subcutaneous

adipose tissue (SAT) depots and deep BAT tissue located proximal to the carotid sheath (*n* = 10 for each tissue). Tissue processing, RNA isolation, and analysis of gene expression has been previously described[75]. Briefly, analysis of gene expression using GeneChIPÒ PrimeView (Affymetrix, Santa Clara, CA) was performed on matched biopsies as previously described[76]. RNA was isolated from clonal cell lines using Direct-zol RNA MiniPrep kit (Zymo Research, Irvine, CA) according to the manufacturer's instructions. The quality of total RNA was evaluated by A260/A280 ratio, which was within the value of 1.9 to 2.0 defined as high quality total RNA. Biotin-labeled cRNA was synthesized, purified and fragmented using GeneChip 3'IVT Express Kit (Affymetrix, Santa Clara, CA). Integrity and fragmented cRNA was assessed by running aliquots on the Agilent 2100 Bioanalyzer prior to proceeding further. The high quality cRNA meets the following criteria: the A260/A280 ratio should fall within the value of 1.9 to 2.0; the 28S/18S RNA bands (from the gel) should be crisp and the intensity of the 28S band should be roughly twice the intensity of the 18S band. Array hybridization and scanning were performed by the Advanced Genomics and Genetics Core of Joslin Diabetes Center according to established methods. Microarray data were normalized using robust multi-array average (RMA), which placed it on a log-2 scale. All subjects gave informed consent prior to taking part in the study. This study followed the institutional guidelines of and was approved by the Human Studies Institutional Review Boards of Beth Israel Deaconess Medical Center and Joslin Diabetes Center

Second cohort – UTMB Washington University adipose tissue cohort: Twenty-three men and women with overweight or obesity (age 41 ± 12 years, BMI 31.0 ± 3 kg/m^2) were enrolled in two clinical trials (NCT02786251 and NCT01791114) performed to determine the role of BAT in metabolic regulation in people. All participants completed a comprehensive screening evaluation that included a medical history and physical examination, standard blood tests, and an oral glucose tolerance test. Potential participants were excluded if they had diabetes or other serious diseases, smoked cigarettes, consumed excessive alcohol, were pregnant or lactating, or had metal implants that interfered with the imaging procedures. The studies were approved by the Institutional Review Board of the University of Texas Medical Branch (UTMB) in Galveston and the Washington University School of Medicine in St. Louis. Written informed consent was obtained from all subjects before their participation. Each participant completed a cold exposure study visit to assess BAT volume and activity and to obtain supraclavicular adipose tissue biopsies. During this visit, a standard cooling protocol was performed to maximize non-shivering thermogenesis[77-79]. After 6 hours of mild exposure to cold (~20^{o}C), an ^{18}F-fluoro-deoxy-glucose (^{18}F-FDG)-positron emission tomography-computed tomography (PET/CT) scan was performed to determine BAT characteristics (volume and activity)[77]. Adipose tissue samples from the supraclavicular area - where BAT is primary localized in humans - obtained using a PET/CT-guided percutaneous needle biopsy technique[80].

Adipose tissue processing and RNA sequencing analysis: Approximately 100 mg of adipose tissue was used for extraction of RNA using the RNeasy Lipid Tissue Mini Kit (Qiagen Inc., Valencia, CA) including an on-column DNAse digestion step. RNA sequencing libraries were generated using the Illumina TruSeq Stranded Total RNA Library Prep Gold with TruSeq Unique Dual Indexes (Illumina, San Diego, CA).

Samples were processed following manufacturer's instructions, except modifying RNA shear time to five minutes. Resulting libraries were multiplexed and sequenced with 75 base pair (bp) single reads (SR75) to a depth of approximately 25 million reads per sample on an Illumina HiSeq 4000. Samples were demultiplexed using bcl2fastq v2.20 Conversion Software (Illumina, San Diego, CA).

Third cohort – Danish adult neck adipose tissue cohort: Adipose tissue biopsies from the superficial (subcutaneous and subplatysmal) neck fat and deep (carotid sheath, longus colli, and prevertebral) neck fat were collected during surgery[81]. None of the subjects had diabetes nor were they administered β-adrenergic antagonists. All biopsies were collected during winter and early spring and were instantly frozen in liquid nitrogen. Only paired biopsies from SAT and BAT of the same subjects were used for associations (n = 73). All study participants gave informed written consent. The study was approved by the Central Denmark Region ethics committee and was performed in accordance with the Declaration of Helsinki. *CKB*, *ALPL*, *ADRA1A,* and *UCP1* mRNA expression was analyzed using RT-qPCR as described above.

Statistical analyses

Statistical analyses were performed with GraphPad Prism 9. Data analysis was performed using Microsoft Office Excel 2021 (version 16.56). Data were expressed as mean ± s.e.m. Unpaired two-tailed Student's t-test for pairwise comparison, one-way ANOVA and two-way ANOVA for multiple comparisons involving two independent variables, and Pearson correlation for linear regression, were used to calculate P values to determine statistical differences. Significance was considered as $P < 0.05$. Mice were randomly assigned to treatment groups for in vivo studies. n values represent independent biological replicates for cell experiments or individual mice for in vivo experiments. Specific details of the n value are noted in each figure legend.

Declarations

Acknowledgements

We thank all members of the Kazak laboratory for critical reading of the manuscript. We thank Jennifer Estall for providing *Ppargc1a*$^{fl/fl}$ mice. This work was supported by a Canadian Institutes of Health Research (CIHR) grant (PJT-159529), a Natural Sciences and Engineering Research Council of Canada (NSERC) Discovery Grant, and the Canadian Foundation for Innovation John R. Evans Leaders Fund (37919) (to L.K.); a Wellcome Trust Senior Research Fellowship (212313/Z/18/Z to D.C.); a CIHR postdoctoral fellowship (to J.F.R.); a NIH grant (K01DK111714, to M.D.L.), a Canderel studentship and a Rolande and Marcel Gosselin Graduate studentship (to M.F.H.); a Canderel studentship (to C.B.D.); and an MRC IMPACT PhD studentship (to E.T.). L.K. is a Canada Research Chair in Adipocyte Biology.

Author contributions: L.K. and J.F.R. conceived the project and designed the experiments. J.F.R., C.S., D.M.L., M.F.H., A.R., C.B.D., J.B., and B.S. performed most of the experiments. O.S.J. performed unilateral BAT denervation's with supervision from Z.G.H. A.R.A. performed experiments with *Ebf1/2* mice with

supervision from P.S.. A.K. provided *Esrra/g*^{AdipoqCre} mice. J.F.R. and C.S. performed ChIP-qPCR experiments with supervision from V.G. J.F.R., C.S., and J.C. conducted ATAC-sequencing. A.P. analyzed RNA-sequencing. A.P., W.A.P., and I.H. analyzed ATAC-sequencing. M.D.L., Y.Z., A.P.W., M.C., S.K., L.S., A.M.C., S.B.P., N.J., and Y.T. harvested and conducted gene expression analyses of human adipose tissues. S.L.O. and E.T. performed BRET-based miniG subtype recruitment assays with supervision from D.C. L.K. wrote the manuscript and supervised the project.

Competing interests: The authors declare no competing interests.

Additional information: Supplementary information is available for this paper. Correspondence and requests for materials should be addressed to lawrence.kazak@mcgill.ca.

Data availability: All data are available in the main article or the supplementary information, and from the corresponding author upon reasonable request. Source data are provided with this paper.

References

1 Cannon, B. & Nedergaard, J. Nonshivering thermogenesis and its adequate measurement in metabolic studies. *J Exp Biol* **214**, 242-253, doi:10.1242/jeb.050989 (2011).

2 Shao, M. & Gupta, R. K. Transcriptional brakes on the road to adipocyte thermogenesis. *Biochim Biophys Acta Mol Cell Biol Lipids* **1864**, 20-28, doi:10.1016/j.bbalip.2018.05.010 (2019).

3 Rahbani, J. F. *et al.* Creatine kinase B controls futile creatine cycling in thermogenic fat. *Nature* **590**, 480-485, doi:10.1038/s41586-021-03221-y (2021).

4 Sun, Y. *et al.* Mitochondrial TNAP controls thermogenesis by hydrolysis of phosphocreatine. *Nature*, doi:10.1038/s41586-021-03533-z (2021).

5 Derry, D. M., Schonbaum, E. & Steiner, G. Two sympathetic nerve supplies to brown adipose tissue of the rat. *Can J Physiol Pharmacol* **47**, 57-63, doi:10.1139/y69-010 (1969).

6 Hull, D. & Segall, M. M. Sympathetic nervous control of brown adipose tissue and heat production in the new-born rabbit. *J Physiol* **181**, 458-467, doi:10.1113/jphysiol.1965.sp007774 (1965).

7 Hsieh, A. C. & Carlson, L. D. Role of adrenaline and noradrenaline in chemical regulation of heat production. *Am J Physiol* **190**, 243-246, doi:10.1152/ajplegacy.1957.190.2.243 (1957).

8 Depocas, F. The calorigenic response of cold-acclimated white rats to infused noradrenaline. *Can J Biochem Physiol* **38**, 107-114 (1960).

9 Chi, J. *et al.* Three-Dimensional Adipose Tissue Imaging Reveals Regional Variation in Beige Fat Biogenesis and PRDM16-Dependent Sympathetic Neurite Density. *Cell Metab* **27**, 226-236 e223, doi:10.1016/j.cmet.2017.12.011 (2018).

10 Cannon, B. & Nedergaard, J. Brown adipose tissue: function and physiological significance. *Physiol Rev* **84**, 277-359, doi:10.1152/physrev.00015.2003 (2004).

11 Moser, C. *et al.* Quantification of adipocyte numbers following adipose tissue remodeling. *Cell Rep* **35**, 109023, doi:10.1016/j.celrep.2021.109023 (2021).

12 Sanchez-Gurmaches, J. *et al.* Brown Fat AKT2 Is a Cold-Induced Kinase that Stimulates ChREBP-Mediated De Novo Lipogenesis to Optimize Fuel Storage and Thermogenesis. *Cell Metab* **27**, 195-209 e196, doi:10.1016/j.cmet.2017.10.008 (2018).

13 Blondin, D. P. *et al.* Human Brown Adipocyte Thermogenesis Is Driven by beta2-AR Stimulation. *Cell Metab* **32**, 287-300 e287, doi:10.1016/j.cmet.2020.07.005 (2020).

14 Cero, C. *et al.* beta3-Adrenergic receptors regulate human brown/beige adipocyte lipolysis and thermogenesis. *JCI Insight* **6**, doi:10.1172/jci.insight.139160 (2021).

15 Collins, S. beta-Adrenoceptor Signaling Networks in Adipocytes for Recruiting Stored Fat and Energy Expenditure. *Front Endocrinol (Lausanne)* **2**, 102, doi:10.3389/fendo.2011.00102 (2011).

16 Keinan, O. *et al.* Glycogen metabolism links glucose homeostasis to thermogenesis in adipocytes. *Nature* **599**, 296-301, doi:10.1038/s41586-021-04019-8 (2021).

17 Panic, V. *et al.* Mitochondrial pyruvate carrier is required for optimal brown fat thermogenesis. *Elife* **9**, doi:10.7554/eLife.52558 (2020).

18 Schreiber, R. *et al.* Cold-Induced Thermogenesis Depends on ATGL-Mediated Lipolysis in Cardiac Muscle, but Not Brown Adipose Tissue. *Cell Metab* **26**, 753-763 e757, doi:10.1016/j.cmet.2017.09.004 (2017).

19 Shin, H. *et al.* Lipolysis in Brown Adipocytes Is Not Essential for Cold-Induced Thermogenesis in Mice. *Cell Metab* **26**, 764-777 e765, doi:10.1016/j.cmet.2017.09.002 (2017).

20 Bachman, E. S. *et al.* betaAR signaling required for diet-induced thermogenesis and obesity resistance. *Science* **297**, 843-845, doi:10.1126/science.1073160 (2002).

21 Fink, S. A. & Williams, J. A. Adrenergic receptors mediating depolarization in brown adipose tissue. *Am J Physiol* **231**, 700-706, doi:10.1152/ajplegacy.1976.231.3.700 (1976).

22 Sveidahl Johansen, O. *et al.* Lipolysis drives expression of the constitutively active receptor GPR3 to induce adipose thermogenesis. *Cell* **184**, 3502-3518 e3533, doi:10.1016/j.cell.2021.04.037 (2021).

23 Long, J. Z. *et al.* A smooth muscle-like origin for beige adipocytes. *Cell Metab* **19**, 810-820, doi:10.1016/j.cmet.2014.03.025 (2014).

24 Roh, H. C. *et al.* Simultaneous Transcriptional and Epigenomic Profiling from Specific Cell Types within Heterogeneous Tissues In Vivo. *Cell Rep* **18**, 1048-1061, doi:10.1016/j.celrep.2016.12.087 (2017).

25 Puigserver, P. *et al.* A cold-inducible coactivator of nuclear receptors linked to adaptive thermogenesis. *Cell* **92**, 829-839, doi:10.1016/s0092-8674(00)81410-5 (1998).

26 Angueira, A. R. *et al.* Early B Cell Factor Activity Controls Developmental and Adaptive Thermogenic Gene Programming in Adipocytes. *Cell Rep* **30**, 2869-2878 e2864, doi:10.1016/j.celrep.2020.02.023 (2020).

27 Brown, E. L. *et al.* Estrogen-Related Receptors Mediate the Adaptive Response of Brown Adipose Tissue to Adrenergic Stimulation. *iScience* **2**, 221-237, doi:10.1016/j.isci.2018.03.005 (2018).

28 Emmett, M. J. *et al.* Histone deacetylase 3 prepares brown adipose tissue for acute thermogenic challenge. *Nature* **546**, 544-548, doi:10.1038/nature22819 (2017).

29 Kopecky, J. *et al.* Synthesis of mitochondrial uncoupling protein in brown adipocytes differentiated in cell culture. *J Biol Chem* **265**, 22204-22209 (1990).

30 Rehnmark, S., Nechad, M., Herron, D., Cannon, B. & Nedergaard, J. Alpha- and beta-adrenergic induction of the expression of the uncoupling protein thermogenin in brown adipocytes differentiated in culture. *J Biol Chem* **265**, 16464-16471 (1990).

31 Klaus, S. *et al.* Characterization of the novel brown adipocyte cell line HIB 1B. Adrenergic pathways involved in regulation of uncoupling protein gene expression. *J Cell Sci* **107 (Pt 1)**, 313-319 (1994).

32 Sondergaard, E. *et al.* Chronic adrenergic stimulation induces brown adipose tissue differentiation in visceral adipose tissue. *Diabet Med* **32**, e4-8, doi:10.1111/dme.12595 (2015).

33 Zhao, J., Cannon, B. & Nedergaard, J. alpha1-Adrenergic stimulation potentiates the thermogenic action of beta3-adrenoreceptor-generated cAMP in brown fat cells. *J Biol Chem* **272**, 32847-32856, doi:10.1074/jbc.272.52.32847 (1997).

34 Alexander, G. M. *et al.* Remote control of neuronal activity in transgenic mice expressing evolved G protein-coupled receptors. *Neuron* **63**, 27-39, doi:10.1016/j.neuron.2009.06.014 (2009).

35 Zhu, H. *et al.* Cre-dependent DREADD (Designer Receptors Exclusively Activated by Designer Drugs) mice. *Genesis* **54**, 439-446, doi:10.1002/dvg.22949 (2016).

36 Nagai, Y. *et al.* Deschloroclozapine, a potent and selective chemogenetic actuator enables rapid neuronal and behavioral modulations in mice and monkeys. *Nat Neurosci* **23**, 1157-1167, doi:10.1038/s41593-020-0661-3 (2020).

37 Mohell, N., Svartengren, J. & Cannon, B. Identification of [3H]prazosin binding sites in crude membranes and isolated cells of brown adipose tissue as alpha 1-adrenergic receptors. *Eur J Pharmacol* **92**, 15-25, doi:10.1016/0014-2999(83)90103-6 (1983).

38 Schimmel, R. J., McCarthy, L. & McMahon, K. K. Alpha 1-adrenergic stimulation of hamster brown adipocyte respiration. *Am J Physiol* **244**, C362-368, doi:10.1152/ajpcell.1983.244.5.C362 (1983).

39 Rokosh, D. G. *et al.* Distribution of alpha 1C-adrenergic receptor mRNA in adult rat tissues by RNase protection assay and comparison with alpha 1B and alpha 1D. *Biochem Biophys Res Commun* **200**, 1177-1184, doi:10.1006/bbrc.1994.1575 (1994).

40 Klepac, K. *et al.* The Gq signalling pathway inhibits brown and beige adipose tissue. *Nat Commun* **7**, 10895, doi:10.1038/ncomms10895 (2016).

41 Blondin, D. P. *et al.* Increased brown adipose tissue oxidative capacity in cold-acclimated humans. *J Clin Endocrinol Metab* **99**, E438-446, doi:10.1210/jc.2013-3901 (2014).

42 Lee, P. *et al.* Temperature-acclimated brown adipose tissue modulates insulin sensitivity in humans. *Diabetes* **63**, 3686-3698, doi:10.2337/db14-0513 (2014).

43 Matsushita, M. *et al.* Impact of brown adipose tissue on body fatness and glucose metabolism in healthy humans. *Int J Obes (Lond)* **38**, 812-817, doi:10.1038/ijo.2013.206 (2014).

44 Becher, T. *et al.* Brown adipose tissue is associated with cardiometabolic health. *Nat Med* **27**, 58-65, doi:10.1038/s41591-020-1126-7 (2021).

45 Cohen, P. *et al.* Ablation of PRDM16 and beige adipose causes metabolic dysfunction and a subcutaneous to visceral fat switch. *Cell* **156**, 304-316, doi:10.1016/j.cell.2013.12.021 (2014).

46 Lowell, B. B. *et al.* Development of obesity in transgenic mice after genetic ablation of brown adipose tissue. *Nature* **366**, 740-742, doi:10.1038/366740a0 (1993).

47 Rothwell, N. J. & Stock, M. J. A role for brown adipose tissue in diet-induced thermogenesis. *Nature* **281**, 31-35 (1979).

48 Seale, P. *et al.* Prdm16 determines the thermogenic program of subcutaneous white adipose tissue in mice. *J Clin Invest* **121**, 96-105, doi:10.1172/JCI44271 (2011).

49 Bartelt, A. *et al.* Brown adipose tissue activity controls triglyceride clearance. *Nat Med* **17**, 200-205, doi:10.1038/nm.2297 (2011).

50 Woodward, J. A. & Saggerson, E. D. Effect of adenosine deaminase, N6-phenylisopropyladenosine and hypothyroidism on the responsiveness of rat brown adipocytes to noradrenaline. *The Biochemical journal* **238**, 395-403, doi:10.1042/bj2380395 (1986).

51 Rajbhandari, P. *et al.* Single cell analysis reveals immune cell-adipocyte crosstalk regulating the transcription of thermogenic adipocytes. *Elife* **8**, doi:10.7554/eLife.49501 (2019).

52 Song, A. *et al.* Low- and high-thermogenic brown adipocyte subpopulations coexist in murine adipose tissue. *J Clin Invest* **130**, 247-257, doi:10.1172/JCI129167 (2020).

53 Chen, Y. *et al.* Thermal stress induces glycolytic beige fat formation via a myogenic state. *Nature* **565**, 180-185, doi:10.1038/s41586-018-0801-z (2019).

54 Sun, W. *et al.* snRNA-seq reveals a subpopulation of adipocytes that regulates thermogenesis. *Nature* **587**, 98-102, doi:10.1038/s41586-020-2856-x (2020).

55 Angueira, A. R. *et al.* Defining the lineage of thermogenic perivascular adipose tissue. *Nat Metab* **3**, 469-484, doi:10.1038/s42255-021-00380-0 (2021).

56 Shamsi, F. *et al.* Vascular smooth muscle-derived Trpv1(+) progenitors are a source of cold-induced thermogenic adipocytes. *Nat Metab* **3**, 485-495, doi:10.1038/s42255-021-00373-z (2021).

57 Acin-Perez, R. *et al.* Recruitment and remodeling of peridroplet mitochondria in human adipose tissue. *Redox Biol* **46**, 102087, doi:10.1016/j.redox.2021.102087 (2021).

58 Rosenwald, M., Perdikari, A., Rulicke, T. & Wolfrum, C. Bi-directional interconversion of brite and white adipocytes. *Nat Cell Biol* **15**, 659-667, doi:10.1038/ncb2740 (2013).

59 Gan, Z. *et al.* Nuclear receptor/microRNA circuitry links muscle fiber type to energy metabolism. *J Clin Invest* **123**, 2564-2575, doi:10.1172/JCI67652 (2013).

60 Murray, J., Auwerx, J. & Huss, J. M. Impaired myogenesis in estrogen-related receptor gamma (ERRgamma)-deficient skeletal myocytes due to oxidative stress. *FASEB J* **27**, 135-150, doi:10.1096/fj.12-212290 (2013).

61 Chaveroux, C. *et al.* Molecular and genetic crosstalks between mTOR and ERRalpha are key determinants of rapamycin-induced nonalcoholic fatty liver. *Cell Metab* **17**, 586-598, doi:10.1016/j.cmet.2013.03.003 (2013).

62 Bolger, A. M., Lohse, M. & Usadel, B. Trimmomatic: a flexible trimmer for Illumina sequence data. *Bioinformatics* **30**, 2114-2120, doi:10.1093/bioinformatics/btu170 (2014).

63 Dobin, A. *et al.* STAR: ultrafast universal RNA-seq aligner. *Bioinformatics* **29**, 15-21, doi:10.1093/bioinformatics/bts635 (2013).

64 Anders, S., Pyl, P. T. & Huber, W. HTSeq–a Python framework to work with high-throughput sequencing data. *Bioinformatics* **31**, 166-169, doi:10.1093/bioinformatics/btu638 (2015).

65 Robinson, M. D. & Oshlack, A. A scaling normalization method for differential expression analysis of RNA-seq data. *Genome Biol* **11**, R25, doi:10.1186/gb-2010-11-3-r25 (2010).

66 Ritchie, M. E. *et al.* limma powers differential expression analyses for RNA-sequencing and microarray studies. *Nucleic Acids Res* **43**, e47, doi:10.1093/nar/gkv007 (2015).

67 Kuleshov, M. V. *et al.* Enrichr: a comprehensive gene set enrichment analysis web server 2016 update. *Nucleic Acids Res* **44**, W90-97, doi:10.1093/nar/gkw377 (2016).

68 Corces, M. R. *et al.* An improved ATAC-seq protocol reduces background and enables interrogation of frozen tissues. *Nat Methods* **14**, 959-962, doi:10.1038/nmeth.4396 (2017).

69 Buenrostro, J. D., Wu, B., Chang, H. Y. & Greenleaf, W. J. ATAC-seq: A Method for Assaying Chromatin Accessibility Genome-Wide. *Curr Protoc Mol Biol* **109**, 21 29 21-21 29 29, doi:10.1002/0471142727.mb2129s109 (2015).

70 Li, H. & Durbin, R. Fast and accurate short read alignment with Burrows-Wheeler transform. *Bioinformatics* **25**, 1754-1760, doi:10.1093/bioinformatics/btp324 (2009).

71 Zhang, Y. *et al.* Model-based analysis of ChIP-Seq (MACS). *Genome Biol* **9**, R137, doi:10.1186/gb-2008-9-9-r137 (2008).

72 Heinz, S. *et al.* Simple combinations of lineage-determining transcription factors prime cis-regulatory elements required for macrophage and B cell identities. *Mol Cell* **38**, 576-589, doi:10.1016/j.molcel.2010.05.004 (2010).

73 Shen, L., Shao, N., Liu, X. & Nestler, E. ngs.plot: Quick mining and visualization of next-generation sequencing data by integrating genomic databases. *BMC Genomics* **15**, 284, doi:10.1186/1471-2164-15-284 (2014).

74 Fischer, A. W., Schlein, C., Cannon, B., Heeren, J. & Nedergaard, J. Intact innervation is essential for diet-induced recruitment of brown adipose tissue. *Am J Physiol Endocrinol Metab* **316**, E487-E503, doi:10.1152/ajpendo.00443.2018 (2019).

75 Xue, R. *et al.* Clonal analyses and gene profiling identify genetic biomarkers of the thermogenic potential of human brown and white preadipocytes. *Nat Med* **21**, 760-768, doi:10.1038/nm.3881 (2015).

76 Cypess, A. M. *et al.* Anatomical localization, gene expression profiling and functional characterization of adult human neck brown fat. *Nat Med* **19**, 635-639, doi:10.1038/nm.3112 (2013).

77 Chondronikola, M. *et al.* Brown adipose tissue improves whole-body glucose homeostasis and insulin sensitivity in humans. *Diabetes* **63**, 4089-4099, doi:10.2337/db14-0746 (2014).

78 Chondronikola, M. *et al.* Brown Adipose Tissue Activation Is Linked to Distinct Systemic Effects on Lipid Metabolism in Humans. *Cell Metab* **23**, 1200-1206, doi:10.1016/j.cmet.2016.04.029 (2016).

79 Yamaguchi, S. *et al.* Adipose tissue NAD(+) biosynthesis is required for regulating adaptive thermogenesis and whole-body energy homeostasis in mice. *Proc Natl Acad Sci U S A* **116**, 23822-23828, doi:10.1073/pnas.1909917116 (2019).

80 Chondronikola, M. *et al.* A percutaneous needle biopsy technique for sampling the supraclavicular brown adipose tissue depot of humans. *Int J Obes (Lond)* **39**, 1561-1564, doi:10.1038/ijo.2015.76 (2015).

81 Breining, P. *et al.* High expression of organic cation transporter 3 in human BAT-like adipocytes. Implications for extraneuronal norepinephrine uptake. *Mol Cell Endocrinol* **443**, 15-22, doi:10.1016/j.mce.2016.12.024 (2017).

Figures

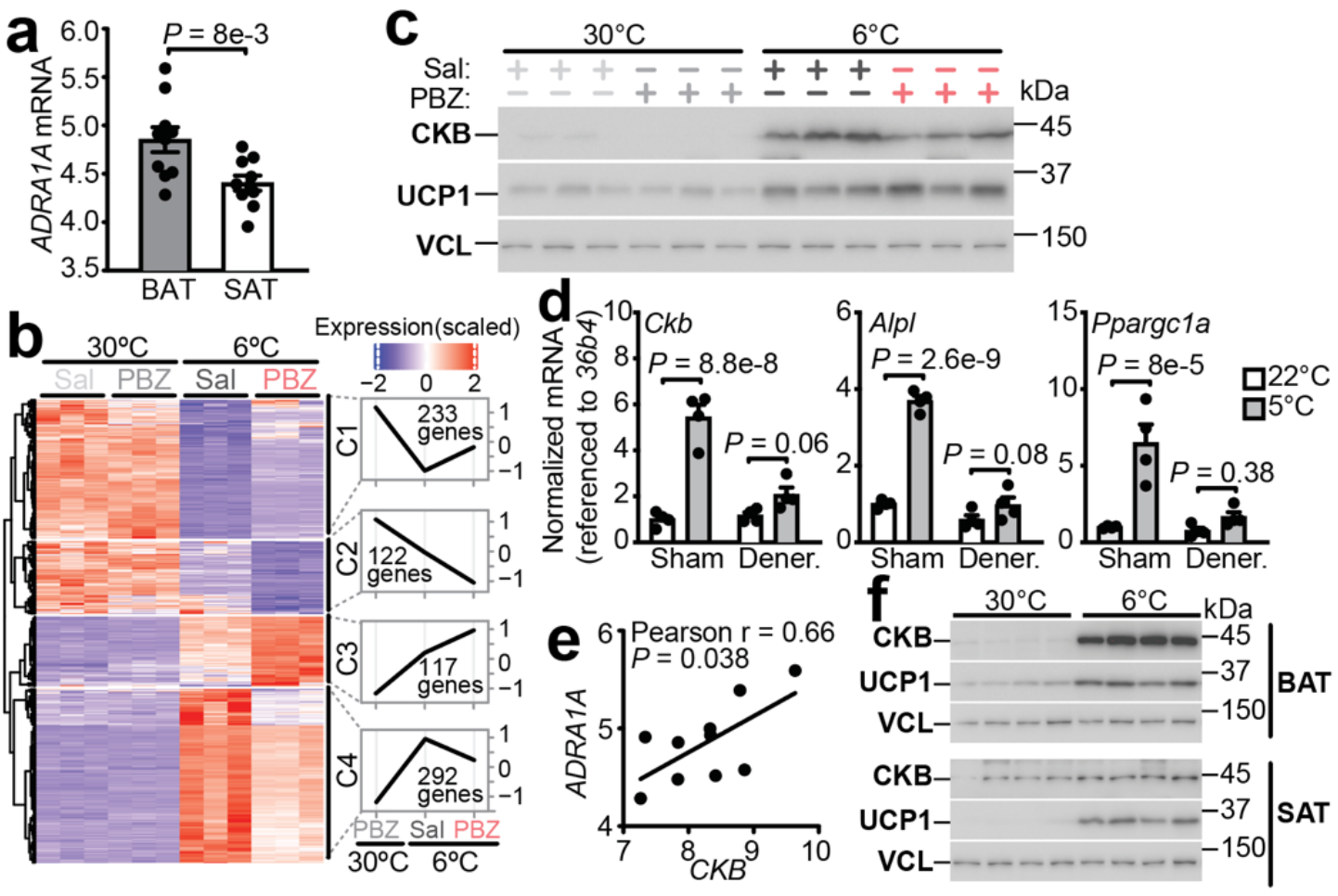

Figure 1

CKB expression is regulated by a-adrenergic receptor signaling. a, Relative mRNA expression of *ADRA1A* from human BAT (n = 10) and paired SAT (n = 10), first cohort. **b,** Heatmap of patterns of gene expression

from BAT of wild-type male mice (C57BL6/N, 6-8 weeks of age), reared at 22°C, housed at 30°C for 5 days and then subjected to 30°C or 6°C at zeitgeber time 4 (ZT4) (*n* = 3 per group). 1 hour prior to onset of 6°C exposure (ZT3), mice were injected intraperitoneally (i.p.) with PBZ (5 mg kg^{-1}) or saline (Sal). BAT was harvested 24 hours after onset of 6°C exposure. Heatmap was constructed using unsupervised hierarchical clustering of the Differentially Expressed Genes (DEGs) in 6°C+Sal vs 6°C+PBZ (FDR < 0.1 using 6°C+Sal as baseline). DEGs were further filtered by comparing 6°C+Sal vs 30°C+Sal or 6°C+PBZ vs 30°C+Sal (log2FC > 1 and FDR < 0.01). To the right of the heatmap is the mean expression levels (scaled) of DEGs in each of the 4 clusters. Complete list of DEGs and their clusters can be found in Extended Data Table 1. **c,** Western blot of BAT from mice treated as in b. **d,** RT-qPCR analysis of sham-operated (Sham) or denervated (Dener.) BAT lobes of mice exposed to 22°C or 5°C for 24 hours (*n* = 4 per group). **e,** Pearson correlation of *CKB* mRNA with *ADRA1A* in human BAT, first cohort (*n* = 10). **f,** Western blot from BAT (top) and SAT (bottom) of male wild-type mice (C57BL6/N, 6-8 weeks of age) reared at 22°C, housed at 30°C for 5 days and then subjected to 30°C or 6°C for 48 hours**.** Data are presented as mean ± s.e.m. of biologically independent samples. **a,** two-tailed student's *t*-tests; **d,** One-way ANOVA (Fisher's LSD); **e,** Pearson correlation**.**

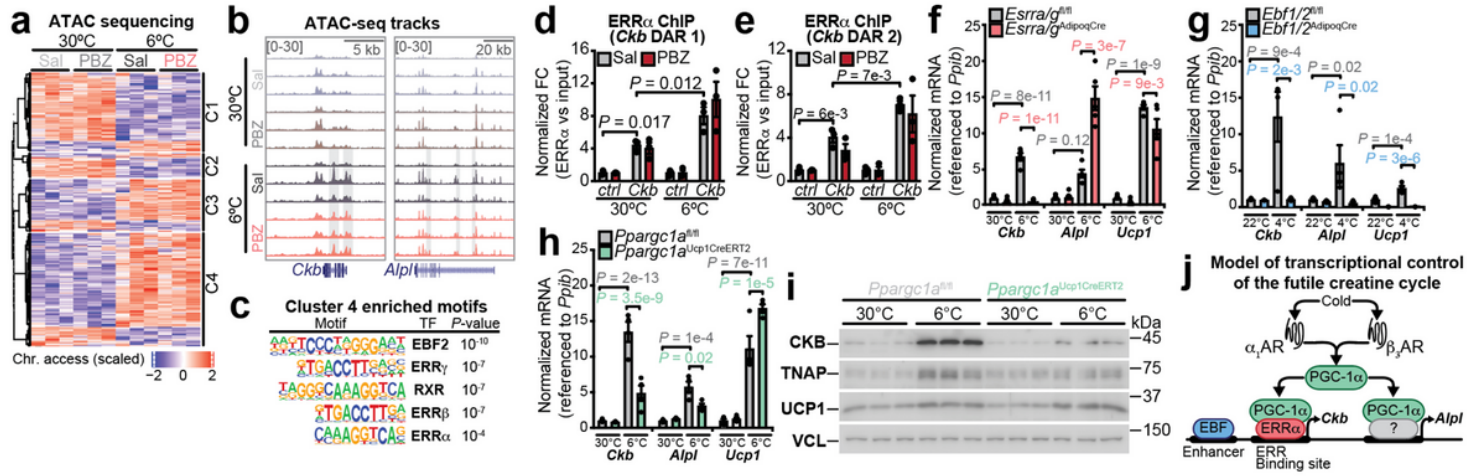

Figure 2

Transcriptional regulation of futile creatine cycling genes. a, Heatmap showing ATAC-seq density of DARs proximal to genes from Fig. 1c (*n* = 3 per group). **b,** ATAC-seq tracks at *Ckb* and *Alpl* loci. Gray shading represents cold-stimulated DARs. **c,** Motifs of transcription factors enriched at DARs proximal to Cluster 4 genes, and present at DARs proximal to both *Ckb* and *Alpl*. **d, e,** Chromatin immunoprecipitation coupled to qPCR (ChIP-qPCR) of ERRα bound to *Ckb* (**d**) DAR 1: chr12:111672017-111672490 and (**e**) DAR 2: chr12:111670556-111670909) (*n* = 3 per group). **f-h,** RT-qPCR from BAT of (**f**) female *Esrra/g*^{AdipoqCre} and *Esrra/g*$^{fl/fl}$ (*n* = 5 per group) (BAT was harvested 24 hours after onset of 6°C exposure); (**g**) male *Ebf1/2*^{AdipoqCre} and *Ebf1/2*$^{fl/fl}$ (*n* = 3-4 per group) (BAT was harvested 7 days after onset of 4°C exposure), and (**h**) male *Ppargc1a*^{Ucp1CreERT2} and *Ppargc1a*$^{fl/fl}$ (*n* = 4 per group) mice (6-10 weeks of age) (BAT was harvested 24 hours after onset of 6°C exposure). **i,** Western blot of BAT from *Ppargc1a*^{Ucp1CreERT2} and *Ppargc1a*$^{fl/fl}$ female mice reared at 22°C, housed at 30°C for 5 days and then subjected to 30°C or 6°C at

zeitgeber time 4 (ZT4). BAT was harvested 48 hours after onset of 6°C exposure. **j,** Model of transcriptional control of the futile creatine cycle. Data are presented as mean ± s.e.m. of biologically independent samples. **d-h,** Two-way ANOVA (Fisher's LSD).

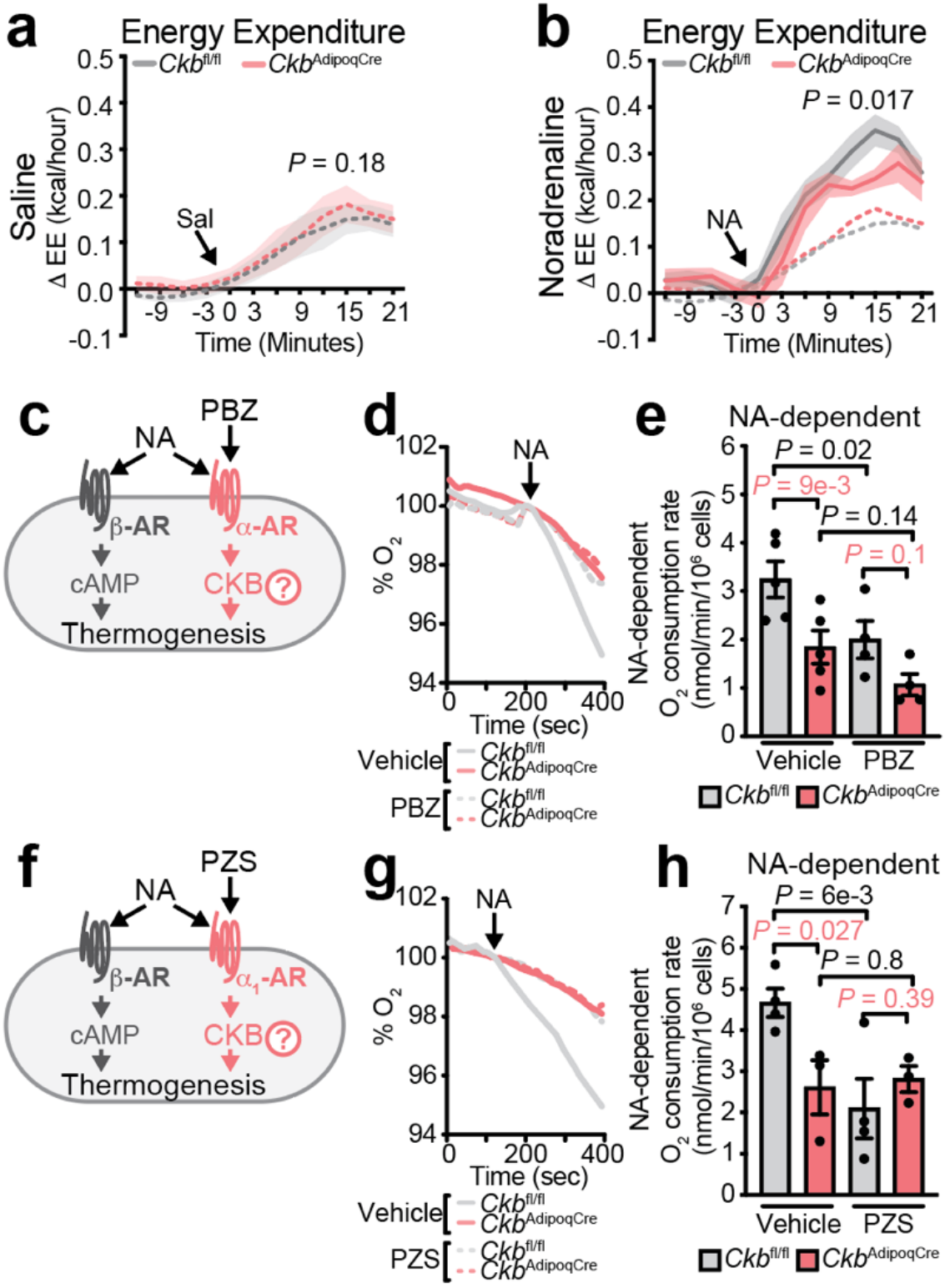

Figure 3

NA-stimulated thermogenesis requires a_1AR signaling and CKB. a-b, Energy expenditure (EE) of *Ckb*$^{fl/fl}$ and *Ckb*^{AdipoqCre} male mice (n = 8 per group) reared at 22°C and then housed for 5 days at 30°C prior to administration of (**a**) saline (Sal) or (**b**) noradrenaline (NA, 1 mg kg^{-1}). **c, f,** Cartoon of approach to determine if (**c**) aAR or (**f**) a_1AR signaling and CKB are necessary for NA-stimulated brown adipocyte thermogenesis. **d, g,** Representative basal and NA-stimulated (0.1 mM) oxygen consumption trace of freshly isolated *Ckb*$^{fl/fl}$ and *Ckb*^{AdipoqCre} brown adipocytes, treated with (**d**) PBZ (1 mM) or (**g**) PZS (1 mM) both compared to vehicle control. The time of NA addition was normalized to 100%. **e, h,** NA-stimulated oxygen consumption rates (above basal) of freshly isolated *Ckb*$^{fl/fl}$ and *Ckb*^{AdipoqCre} brown adipocytes, treated with (**e**) PBZ (*n* = 5).or (**h**) PZS (*n* = 4). both compared to vehicle control. Data are presented as mean ± s.e.m. of biologically independent samples. **a, b,** Two-way ANOVA (Fisher's LSD) from minutes 0 to 21; **e, h,** One-way ANOVA (Fisher's LSD).

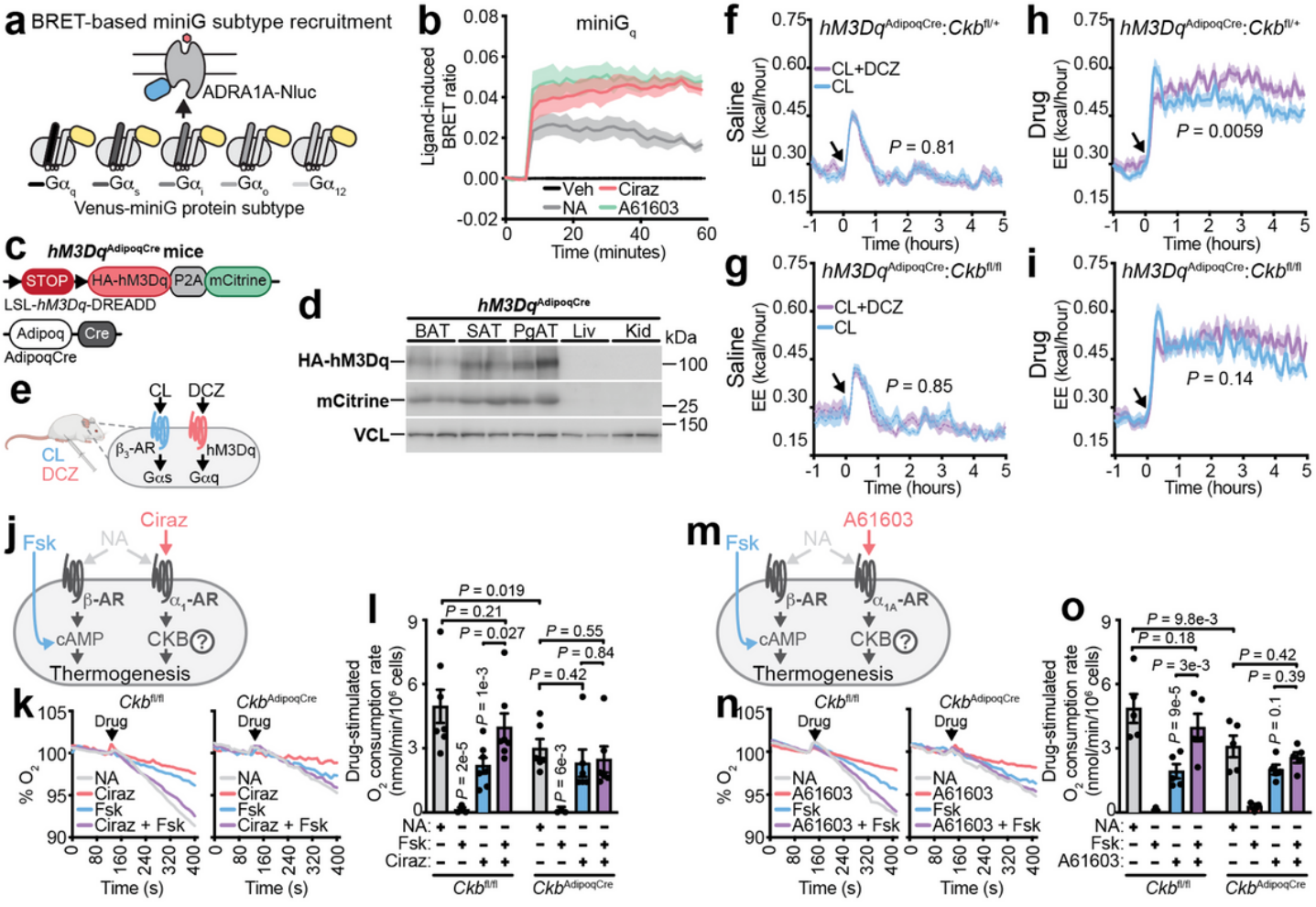

Figure 4

Thermogenesis by combined a_{1A}AR and cAMP signaling genetically requires *Ckb*. a, Schematic of bioluminescence resonance energy transfer (BRET)-based miniG subtype recruitment assay. **b,** Agonist-

induced BRET between ADRA1A-tagged Nano Luciferase (ADRA1A-Nluc) and Venus-tagged miniGa_q protein sensor in immortalized brown adipocytes (*n* = 3 per group, each agonist/vehicle performed in triplicate). Noradrenaline (NA), cirazoline, and A61603 were all used at 1 mM. **c,** Cartoon of *hM3Dq*^{AdipoqCre} mouse construction. **d,** Western blot of BAT, SAT, perigonadal adipose tissue (PgAT), liver (Liv) and kidney (Kid) from *hM3Dq*^{AdipoqCre} mice. **e,** Schematic of activation of Ga_s and Ga_q signaling in adipocytes from *hM3Dq*^{AdipoqCre} mice. **f, h**, Energy expenditure (EE) of *hM3Dq*^{AdipoqCre}:*Ckb*$^{fl/+}$ mice reared at 22°C and then housed for 5 days at 30°C prior to administration of (**f**) saline or (**h**) CL 316,243 (CL, 0.5 mg kg^{-1}) (*n* = 24: *n* = 16 males, *n* = 8 females) or CL + DCZ (both at 0.5 mg kg^{-1}) (*n* = 25: *n* = 17 males, *n* = 8 females). **g-i**, EE of *hM3Dq*^{AdipoqCre}:*Ckb*$^{fl/fl}$ mice reared at 22°C and then housed for 5 days at 30°C prior to administration of (**g**) saline or (**i**) CL (0.5 mg kg^{-1}) (*n* = 15: *n* = 7 males, *n* = 8 females) or CL + DCZ (both at 0.5 mg kg^{-1}) (*n* = 15: *n* = 7 males, *n* = 8 females). **j,** Cartoon of approach to study brown adipocyte-intrinsic thermogenesis by individual and combined activation of a_1AR and cAMP signaling. **k,** Representative oxygen consumption trace of freshly isolated *Ckb*$^{fl/fl}$ and *Ckb*^{AdipoqCre} brown adipocytes, treated with NA (0.1 mM), cirazoline (a_1AR agonist, Ciraz, 1 mM), forskolin (Fsk, 3 mM), or Ciraz+Fsk. The time of drug addition was normalized to 100%. **l,** Oxygen consumption rates from multiple experiments of brown adipocytes treated as in k (*n* = 3-7 per group). **m,** Cartoon of approach to study brown adipocyte-intrinsic thermogenesis by individual and combined activation of a_{1A}AR and cAMP signaling. **n,** Representative oxygen consumption trace of freshly isolated *Ckb*$^{fl/fl}$ and *Ckb*^{AdipoqCre} brown adipocytes, treated with NA, A16063 (a_{1A}AR agonist, 1 mM), Fsk, or A16063+Fsk. The time of drug addition was normalized to 100%. **o,** Oxygen consumption rates from multiple experiments of brown adipocytes treated as in n (*n* = 3-5 per group). Data are presented as mean ± s.e.m. of biologically independent samples. **f, g,** Two-way ANOVA (Fisher's LSD) from hours -1 to 5; **h, i,** Two-way ANOVA (Fisher's LSD) from hours 1 to 5 (1 hour after injection was chosen because the stress response had subsided); **l, o,** One-way ANOVA (Fisher's LSD).

Supplementary Files

This is a list of supplementary files associated with this preprint. Click to download.

- ExtendedDataFigures.docx